

AUS Repository

Evaluation of fiber reinforced polymer bars under compression: experiments and finite element simulations

Item Type	Thesis
Authors	Al Najmi, Laith Abdul-Qader Said
Download date	2026-05-20 17:33:13
Link to Item	http://hdl.handle.net/11073/21358

EVALUATION OF FIBER REINFORCED POLYMER BARS UNDER
COMPRESSION: EXPERIMENTS AND FINITE ELEMENT
SIMULATIONS

by

Laith Abdul-Qader Said Al Najmi

A Thesis Presented to the Faculty of the
American University of Sharjah
College of Engineering
in Partial Fulfillment
of the Requirements
for the Degree of

Master of Science in
Civil Engineering

Sharjah, United Arab Emirates

November 2020

Declaration of Authorship

I declare that this thesis is my own work and, to the best of my knowledge and belief, it does not contain material published or written by a third party, except where permission has been obtained and/or appropriately cited through full and accurate referencing.

Signed: Laith Abdul-Qader Said Al Najmi

Date: 7 / 12 / 2020

The Author controls copyright for this report.
Material should not be reused without the consent of the author. Due
acknowledgement should be made where appropriate.

© Year 2020

Laith Abdul-Qader Said Al Najmi

ALL RIGHTS RESERVE

Approval Signatures

We, the undersigned, approve the Master's Thesis of Laith Abdul-Qader Said Al Najmi

Thesis Title: Evaluation of fiber reinforced polymer bars under compression: experiments and finite element simulations.

Date of Defense: 19/11/2020

Name, Title and Affiliation

Signature

Dr. Farid Abed
Professor, Department of Civil Engineering
Thesis Advisor

Dr. Rami Haweeleh
Professor, Department of Civil Engineering
Thesis Committee Member

Dr. Basil Darras
Associate Professor, Department of Mechanical Engineering
Thesis Committee Member

Dr. Irtishad Ahmed
Head
Department/Program of Civil Engineering

Dr. Lotfi Romdhane
Associate Dean for Graduate Studies and Research
College of Engineering

Dr. Sirin Tekinay
Dean
College of Engineering

Dr. Mohamed El-Tarhuni
Vice Provost for Graduate Studies
Office of Graduate Studies

Acknowledgment

First and foremost, I quote “And the last of our call is Praise be to God, Lord of the Worlds”.

Secondly, A hearty thanks to my Advisor Dr. Faird Abed for spending the time to guide and to help even at irregular times to accommodate me after my office working hours.

Last but not least, to my family; to my parents who have lift me in the previous years to reach where I am now, to my wife who spared all the time and love to support me.

Dedication

To my parents, wife, son and family...

Abstract

The behavior of Fiber-reinforced polymers (FRP) bars under compression is not fully understood yet due to the limited research in this area; therefore, American concrete institute (ACI) does not recommend using FRP bars in compression. However, the long-term durability, weathering resistance, and exceptional mechanical properties of FRP bars justify the need for their use in compression members. The main objectives of this study are to evaluate the mechanical properties of Glass FRP (GFRP) and Basalt FRP (BFRP) bars under compression and examine their performance as main longitudinal reinforcement in reinforced concrete columns. In the first part of this research, a series of static tests were conducted on GFRP and BFRP specimens of different diameters. Steel grips filled with epoxy were used at the top and bottom surfaces of the FRP bar to avoid premature failure at the ends and ensure pure compression. The second part of this research numerically investigated the behavior of FRP-RC columns under concentric and eccentric loading using the mechanical properties of FRP bars obtained experimentally. For this purpose, nonlinear finite element models were developed and verified using the experimental results conducted previously at the AUS construction lab. The verified FE models were then utilized to conduct a parametric analysis to simulate the compressive behavior of concrete columns reinforced with GFRP and BFRP bars. Interaction diagrams were also developed based on the FE analysis considering different design parameters such as the cross-section of the column, type and ratio of longitudinal and lateral reinforcement, and loading eccentricities.

Keywords: *FRP, GFRP, BFRP, ACI, Compression, Columns, FEA, ABAQUS*

Table of Contents

Abstract	6
List of Figures	9
List of Tables	12
List of Abbreviations	13
Chapter 1. Introduction	14
1.1. Overview	14
1.2. Problem Statement	15
1.3. Thesis Objectives	16
1.4. Research Contribution and Significance	16
1.5. Thesis Organization.....	17
Chapter 2. Background and Literature Review.....	18
2.1. Physical and Mechanical Properties of FRP Bars	18
2.2. Literature Review	20
2.2.1. Valuation of FRP under different loading conditions.....	20
2.2.2. Capacity of FRP bars under compression.....	21
2.2.3. Effect of varying loading rate and type on FRP bars under compression.	26
2.2.4. Challenges and observation on concrete columns reinforced with FRP bars.....	27
2.2.5. Challenges and observation on finite element modeling of columns reinforced with FRP.....	29
2.2.6. Evaluation of the mechanical properties of concrete.	33
2.2.7. Failure mechanisms of concrete under different loading rates.	33
2.2.8. Design equations for FRP-RC columns.	34
Chapter 3. Experimental Evaluation of BFRP and GFRP Bars under Compression	37
3.1. Test Material.....	37
3.2. Specimen Design and Preparation.....	38
3.3. Test Matrix	38
3.4. Test Setup and Procedure and Instrumentation Used in the Tests	39
3.5. Experimental Results.....	45
Chapter 4. Evaluation of RC Columns Reinforced with GFRP and BFRP Bars.....	47
4.1. Finite Element Modeling.....	47

4.1.1 Model material.	47
4.1.2 Model geometry.	48
4.1.3 FE model verification.	51
4.1.4 Parametric analysis: Performance of GFRP- and BFRP-RC columns.	54
Chapter 5. Discussion of Results	68
5.1. Effects of Parameters on the Overall Behavior of FRP RC Columns.	68
5.2. Effect of Longitudinal Reinforcement Type and Ratio.	70
5.3. Effect of Cross-Sectional Shape and Dimension	71
5.4. Effect of Transverse Reinforcement Type	72
5.5. Interaction Diagrams	72
5.6. Evaluation of Proposed Design Equations for FRP RC Columns.	74
Chapter 6. Conclusion and Future Work	79
References.	82
Vita.	89

List of Figures

Figure 2.1: Sample test setup by Plevkov et al. [31]	21
Figure 2.2: Sample test setup by Khorramian et al. [32]	22
Figure 2.3: Sample test setup by Khorramian et al. [33]	23
Figure 2.4: Sample test setup by Deitz et al. [34]	24
Figure 2.5: Sample test setup by Khan et al. [35]	25
Figure 2.6: Sample test setup by Thiyagarajan et al. [37]	25
Figure 2.7: The typical geometry by Elchalakani of the FE models of, (a) concentrically loaded columns, (b) eccentrically loaded columns, (c) GPC and OPC concrete beams (d), OPC concrete columns [50].....	30
Figure 2.8: Sketch of RC columns by Elchalakani, (a) concentrically loaded column, (b) eccentrically loaded column, (c) beam. (in mm) [50].....	31
Figure 2.9: Typical FEA results for (a) concentrically loaded columns, (b) eccentrically loaded columns, (c) RC beams [50].....	32
Figure 3.1: FRP bars samples (a) GFRP bar samples (b) BFRP bar samples	37
Figure 3.2: First attempted test setup sketch.....	39
Figure 3.3: First attempted test setup typical one end	40
Figure 3.4: Second attempted setup schematic sketch.....	41
Figure 3.5: Second attempted test setup (a) alignment Tool (b) sample specimens....	41
Figure 3.6: Typical attempted setups 1 and 2 testing outcome (a) typical sample failure (b) typical tilting of samples during testing	42
Figure 3.7: Used test setup sketch.....	43
Figure 3.8: Used test setup.....	43

Figure 3.9: Experimental setup of static loading (a) an overview picture of the testing machine with the bar (b) a focused picture on the bar inside the testing machine	44
Figure 3.10: Apparatus used for cutting the samples.....	44
Figure 3.11: Typical samples failure mode (a) GFRP sample (b) BFRP sample	46
Figure 4.1: (a) Inelastic compressive and (b) tensile behaviors of concrete used in the FE Model.....	48
Figure 4.2: (a) Chosen mesh for the square cross section of (180x180x1100) mm (b) geometry of cage	49
Figure 4.3: (a) mesh configuration and (b) load vs. displacement results for the different element sizes.....	51
Figure 4.4: Experimental column by ElMesalami [61], [62].....	52
Figure 4.5: Columns cross section (in mm) by ElMesalami [61], [62].	53
Figure 4.6: Comparison between experimental and FEA results	53
Figure 4.7: Load vs displacement comparison between experimental work and FE modelling.....	54
Figure 4.8: Rectangular FRP-RC column details: (a) column dimensions (b) cross section of 180 mm x180 mm column (c) cross section of 200 mm x200 mm column	55
Figure 4.9: Circular FRP-RC column detail of 203 mm diameter (a) column dimension (b) cross section	55
Figure 4.10: Load vs. displacement results for columns in Group 1, at the 1% reinforcement ratio.	58
Figure 4.11: Group-1 interaction diagram	59
Figure 4.12: Group-2 interaction diagram	60
Figure 4.13: Group-3 interaction diagram	60
Figure 4.14: Group-4 interaction diagram	61

Figure 4.15: Group-5 interaction diagram	61
Figure 4.16: Group-6 interaction diagram	62
Figure 4.17: Group-7 interaction diagram	62
Figure 4.18: Group-8 interaction diagram	63
Figure 4.19: Group-9 interaction diagram	63
Figure 4.20: Group-10 interaction diagram	64
Figure 4.21: Theoretical as per ACI318 [58] vs experimental interaction diagram for group-1 (1%).....	67
Figure 5.1: Determination of displacements for calculating columns ductility index (graph of column ID S-G180-S00-40 1%).....	70
Figure 5.2: Group-4 force vs displacement For 1% and 8% reinforcement ratio.....	71
Figure 5.3: Rectangular column cross sectional strain diagram	73
Figure 5.4: Group 1 FEA results comparison with proposed short columns equations	74
Figure 5.5: Group 3 FEA results comparison with proposed short columns equations	75
Figure 5.6: Group 4 FEA results comparison with proposed short columns equations	75
Figure 5.7: Group 5 FEA results comparison with proposed short columns equations	76
Figure 5.8: Group 7 FEA results comparison with proposed short columns equations	76
Figure 5.9: Group 8 FEA results comparison with proposed short columns equations	77
Figure 5.10: Group 10 FEA results comparison with proposed short columns equations	77

List of Tables

Table 2.1: Summary of the properties of FRP bars, steel, wood and concrete as reported in previous studies [2], [8]–[10].....	19
Table 2.2: Compressive strength and elastic modulus of FRP bars as reported in previous studies.....	26
Table 2.3: Summary of the design equations presented in the literature for FRP-RC columns	34
Table 3.1: Tensile properties of bars reinforcements [17], [39]	38
Table 3.2: Test matrix	39
Table 3.3: Properties of GFRP reinforcements.....	45
Table 3.4: Properties of BFRP reinforcements	45
Table 4.1: Test matrix, specimens' details and results [61], [62].....	51
Table 4.2: Parametric study groups table.....	57
Table 4.3: Confined concrete strength factors and ductility indices of all concentric columns	65

List of Abbreviations

ACI -	American Concrete Institute
ASTM -	American Society for Testing and Materials
BFRP -	Basalt Fiber-Reinforced Polymer
CFRP -	Carbon Fiber-Reinforced Polymer
CSA -	Canadian Standards Association
FEA -	Finite Element Analysis
FRP -	Fiber-Reinforced Polymer
FE-	Finite Element
GFRP -	Glass Fiber-Reinforced Polymer
RC -	Reinforced Concrete
UTM -	Universal Testing Machine

Chapter 1. Introduction

In recent years, fiber-reinforced polymer (FRP) bars have been used to reinforce concrete members in tension, whereas their contribution in compression has been ignored because of the insufficient number of research. In this chapter, the advantages of FRP bars will be discussed along with examples of their current applications.

1.1. Overview

The main reason behind replacing steel bars with FRP bars in reinforced concrete structures is that steel corrodes with time. Therefore, steel reinforcements require rehabilitation and regular maintenance. Thus, in order to achieve the targeted performance, objectives and properties, a composite material which combines two or more constituents (e.g., Fiber reinforcement and binder or matrix resins) is introduced.

FRP contains two-component composite materials of polymer matrix and a high strength fibers embedded in. The mechanical and physical properties of FRPs are governed by their manufacturing process which affects micro-structural configuration and the properties of their constituents. In which the fibers are dominantly accountable for the mechanical properties, the polymeric matrix transfers the load and provides environmental protection. Additionally, the FRP bars manufacturing process is controlled by the resin. In addition, fillers decrease the cost and may sometimes enhance the performance, providing advantages such as shrinkage control, surface smoothness and crack resistance [1].

There has been substantial research on the development of FRP composites and their innovative applications, and many publications have resulted in an improved structural performance. FRP composites are being endorsed as twenty-first century materials because of their superior corrosion resistance. The original FRP composites used glass fibers (GFRP) which were made available by the growing industry following the second World War. The blend of high strength and stiffness structural fibers combined with lightweight, cost-effective and corrosion resistant polymers results in materials with mechanical characteristics and durability that are much better than any of the both elements alone [2].

Over the last ten years, there has been substantial increase in using FRP composites in construction and in structural engineering. FRP composites have been

recognized to be important for usage in the building of new structures and for rehabilitating old buildings. Indeed, for structural applications where high strength and stiffness to weight ratios are essential, FRP composites are the optimal choice [3]. Nevertheless, the applications of advanced composite materials in civil engineering have been developing slowly, primarily due to economic reasons. This class of materials has been extensively studied and used in the structural and aerospace engineering fields, such as aircraft construction [4]. Their main advantages, such as tailorable design features, and high ratio of strength to weight notably surpass materials of conventional civil engineering. The ACI 440.1R-15, however, does not allow considering the FRP contribution as compressive reinforcement in concrete columns. Although FRP materials can resist compressive load, there are several matters that surrounds using FRP for compression [5].

Compression members are generally handled with extra care during installation and preparation. If the surface of the compression element sample is not completely perpendicular to the fixed end surface or if the loading is not at the centroid of the cross-sectional area of the sample, eccentricity will be induced. Eccentricity will create a moment on the sample, resulting in inaccurate results (underestimated values). Testing an FRP bar under compression with eccentric loading causes the behavior of the bar to change from an axial compression-resisting element to a flexural-resisting element.

1.2. Problem Statement

The construction industry does not usually take the leadership into adopting new technologies, and frequently resists implementing them. Additionally, the present practice of substitution of conventional materials by unconventional composite components in traditional structural systems has shown that the use of unconventional composites in civil construction is difficult to justify, not only in an economical point of view, but also in a structural one. [6]. The new materials should be tested, and their abilities and advantages have to be validated before the new materials can be employed in the field of construction. Furthermore, both structural and economic factors are to be considered during the process of introducing new materials.

Steel reinforcing bars have been used since the early stages of the modern construction era. Despite their competence as structural members, steel reinforcing bars are metallic material that are vulnerable to various environmental conditions, such as

corrosion. Corrosion can degrade a steel bar dramatically and reduce its strength. To counter the effect of corrosive environments, non-metallic reinforcement bars, such as FRP reinforcements, were proposed. However, while steel bars have an advantage of being ductile, FRP bars are brittle, which means that they have linear elastic stress-strain behavior until failure. Thus, the engineering community had to be more stringent with the use of FRP bars. This can be noticed when comparing the factors of safety between ACI 440.1R code and ACI 318.

FRP bars are anisotropic and their implementation is only accepted in some loading cases. FRP bars are now accepted as part of structures where they can resist tensile forces. In contrast, the usage of FRP bars in compression is still not accepted by the engineering community due to the lack of experiments and the belief that FRP bars do not have enough strength to resist compression.

1.3. Thesis Objectives

The main objectives of this research are:

- 1- To evaluate the mechanical properties of GFRP and BFRP bars in compression and their potential of replacing conventional steel reinforcements in columns.
- 2- To develop a finite element model of a reinforced concrete column with FRP bars, using the compression properties of GFRP and BFRP from testing.
- 3- To conduct a parametric study and develop interaction diagrams for GFRP and BFRP RC columns considering different reinforcement ratios, cross-sections and loading eccentricities.

In this research the main parameters are the type of loading, material and diameter of bar, and the fixing arrangement. Experimental tests are conducted to obtain the mechanical properties (strength and elastic modulus) of GFRP and BFRP bars under static compression loadings.

1.4. Research Contribution and Significance

The idea of using FRP bars as compression reinforcement is still new research-wise. Investigating the capability of FRP bars in compression is needed so that they can be accepted and considered in the latest codes for compression members. Few

researchers have studied the behavior of FRP bars under compression, but have not reported solid results to show the reliability of FRP under compression. In this thesis, experimental tests are conducted on GFRP and BFRP bars under static compressive loadings to investigate their behavior under compression. A special test setup and sampling technique is utilized to ensure pure axial loading on the bars to accurately estimate their ultimate strengths and modulus of elasticity. Also, a finite element model of a reinforced concrete column with FRP bars is developed and verified, then utilized to conduct a parametric analysis.

1.5. Thesis Organization

The remainder of the thesis is structured as follows: Chapter 2 presents the literature review and information about both the mechanical and physical properties of FRP bars. This is followed by discussing finite elements modelling and challenges. Chapter 3 outlines the experimental program of this thesis, including details of the bar specimens tested and descriptions of the test set-ups. Chapter 4 describes the FE modelling, definitions and steps and the parametric study. Then, the results of the experimental tests and parametric study are detailed in Chapter 5. Lastly, Chapter 6 offers conclusion of the thesis and suggests future work recommendations.

Chapter 2. Background and Literature Review

In this chapter, the mechanical and physical properties of FRP bars will be discussed, different research in this area will be explained. Then a review of existing research on FE modelling is presented, and then the contribution of this current work to existing literature will also be considered.

2.1. Physical and Mechanical Properties of FRP Bars

The main purpose of FRP bars is to replace or be an alternative option for the steel reinforcement. For that reason, the properties of FRP bars should be compared with the properties of steel bars to assess their advantages and disadvantages.

FRP bars are orthotropic, which means that the mechanical properties obtained from testing FRP bars under tension will not be the same as that obtained under compression. FRP bars consist of high strength fibers such as aramid, basalt, carbon or glass, embedded in a polymer resin such as epoxy [7]. As a result, the theoretical E value in the direction of the fiber would be $E = E_f V_f + E_m V_m$, where E_f is the fiber elastic modulus, V_f is the fiber volume fraction, E_m is the matrix elastic modulus, and $V_m = 1 - V_f$ is the matrix volume fraction. Steel reinforcement bars, on the other hand, are isotropic and assumed to have the same mechanical properties under tension and compression. Also, FRP bars have lower modulus of elasticity and higher ultimate strength compared to steel. The properties of FRP bars are not consistent but dependent on the manufacturing process and quality, which leads to varying FRP properties from one product to another and from one manufacturer to another. Additionally, in terms of thermal conductivity, the high durability of FRPs guarantees much more stable behavior. Consequently, FRP bars do not degrade from aging and weathering, unlike steel which is not considered as durable and corrodes with time [8]. However it is critical for the engineer and manufacturer to be able to prove that a given FRP material system and/or assembly is fire-protected, given the commonly observed limitations of FRPs under fire [8].

Generally, the density of BFRP is around 2750 kg/m³ while the density of GFRP is around 2200 kg/m³ [57]. For BFRP bars, the tensile strength can reach up to 1600 MPa and the tensile modulus of elasticity is around 45 GPa [36]. For GFRP bars,

on the other hand, the tensile strength can reach up to 1200 MPa and the modulus of elasticity can reach up to 69-86 GPa [30], [33].

The main characteristic values for GFRP and BFRP and other well-known construction materials are shown in Table 2.1. Data about FRPs have been elaborated from [2], [8]–[10].

Table 2.1: Summary of the properties of FRP bars, steel, wood and concrete as reported in previous studies [2], [8]–[10]

Characteristics	GFRP	BFRP	Steel	Wood	Concrete
Tensile Strength (MPa)	700 -1200	800-1600	450	70-100	2 to 5
Tensile Modulus of elasticity (GPa)	40-60	40-60	210	Up to 12	Up to 50
Density (kg/m ³)	2200	2750	7500	200-1400	2200

The advantages and disadvantages of reinforcing concrete columns with FRP bars in comparison with conventional steel materials are as detailed below:

Advantages:

- 1- FRP materials are non-corrosive and non-magnetic.
- 2- FRPs are extremely light and strong (high ratio of strength to weight), and comparatively easy to install.
- 3- FRP costs have decreased and FRPs are currently recognized as effective and efficient structural materials.
- 4- FRP materials' thermal conductivity is low.

Disadvantages:

- 1- FRPs are linear-elastic materials (Brittle).
- 2- FRPs have a high initial material cost (without considering life cycle costs).

Since this technology (FRP) is still developing and changes are being frequently made to design documents in order to incorporate recent findings. New codes, such as

American Concrete Institute (ACI-440), Japan Concrete Institute (JCI), and ISIS Canada are being developed.

The main role of fibers is to resist a major percentage of the load acting on the composite system while the role of the matrix is to transfer loads between fibers. Each FRP type has its own mechanical and physical property. Glass fibers have a low cost, a high tensile strength, a high chemical resistance, and a high temperature resistance. However, glass fibers are very sensitive to scratching and have low fatigue resistance. Compared to other fibers, carbon fibers have the highest tensile modulus, an exceptionally high tensile-to-strength ratio, and a high fatigue resistance. Carbon fibers, though, are the most expensive kind of fibers. Aramid fibers are lighter than glass fibers and carbon fibers, have a good resistance to impact loading, and have a high tensile strength, but have a low compressive strength and degrade when exposed to ultraviolet light. Basalt fibers have a very high scratch resistance and are better than glass fibers in terms of thermal stability [11].

2.2. Literature Review

Many studies had also been conducted to evaluate the durability [12]–[15], flexural [16]–[19], and shear [20]–[25] performances of concrete beams reinforced with carbon (CFRP), glass (GFRP), and basalt (BFRP) FRP types of bars. Other studies investigated the effect of high temperatures on the performance of FRP bars [26]. Hybrid reinforcements of steel and FRP bars were also examined for slender beams under flexure [27], [28]. However, limited research has investigated the behavior of FRP bars under compression. Researchers have studied the compression behavior of FRP bars and compared them with tensile properties of different lengths and sample diameters. Different setups were made with varying ways of measurement (strain gauges), methods of fixing the ends as well as strain rates. There is still no concrete evidence in terms of research to show the capability of FRP bars to carry loads under compression. The sample setup for FRP bars under compression will affect the results; parameters such as bar length, fixed ends parts and ends leveling with the surface will change the test results. Thus, bar samples in compression must be handled with care.

2.2.1. Valuation of FRP under different loading conditions. Many studies had been conducted to evaluate the durability [12]–[15], [29], the flexural behavior [16]–[18], and shear behavior [20]–[25] of concrete beams reinforced with various

types of FRP bars. Other studies investigated the effect of high temperatures on the performance of FRP bars [26]. Hybrid reinforcements of steel and FRP bars were also examined for slender beams under flexure [27], [28]. However, limited research was conducted on investigating the compressive response of FRP bars. Elmessalami et al. [30] studied the behavior FRP-reinforced columns. Where a wide-ranging literature review on FRP-reinforced columns was studied in order to improve the understanding of their performance under different loading conditions.

2.2.2. Capacity of FRP bars under compression. Very limited studies have studied the mechanical properties of FRP bars under compression. A study by Plevkov et al. [31] studied the behavior of GFRP and CFRP bars of 10 mm diameter and 50 mm length under compression. The test samples were placed into a special device which consists of two steel couplings and a sleeve, as shown in Figure 2.1 The couplings were fixed with composite glue at the ends of the rods and then placed inside a steel sleeve. In the study, it was observed that CFRP samples failed by buckling. Moreover, the modulus of elasticity was found to be 41 GPa for GFRP bars, which is 67% of that in tension, and 105 GPa for CFRP bars, which is 73% of that in tension.

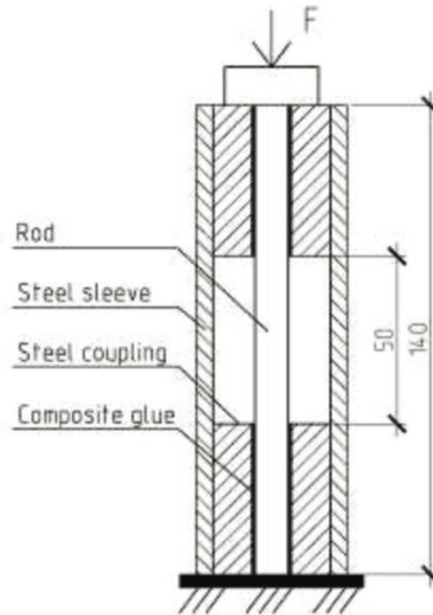


Figure 2.1: Sample test setup by Plevkov et al. [31]

Another study by Khorramian et al. [32], studied the behavior of GFRP bars of 13-, 16- and 19-mm diameters. The length of the GFRP bars was 4 times their diameter

to allow an unsupported length equal to twice of the diameter. A couple of strain gauges were placed at the center of the bar on two opposite sides. For the first and third group, the strain gauges were installed directly on the GFRP bars (applied 16 mm diameter). For the second group, resin was applied at the center of the bars and the strain gauges were attached on the surface of the machined resin instead. Based on the results from these gauges, the average strain value in each GFRP bar was calculated. The alignment was done by installing adhesive anchors with a level as shown in Figure 2.2 The specimens were tested by applying a uniform and monotonic compression force of 0.5 mm/min. Overall, the test results were consistent and the elasticity modulus, strength and proportional limit (effective compressive strain) of the GFRP bars were evaluated. The results highlighted that the GFRP bars' compressive properties are comparable to the tensile properties. The modulus of elasticity values for the 13, 16, and 19 mm diameter bars were 45 GPa, 42 GPa, and 49 GPa, respectively. However, by adding a methodology to find the proportional limit, the test technique might have been improved.

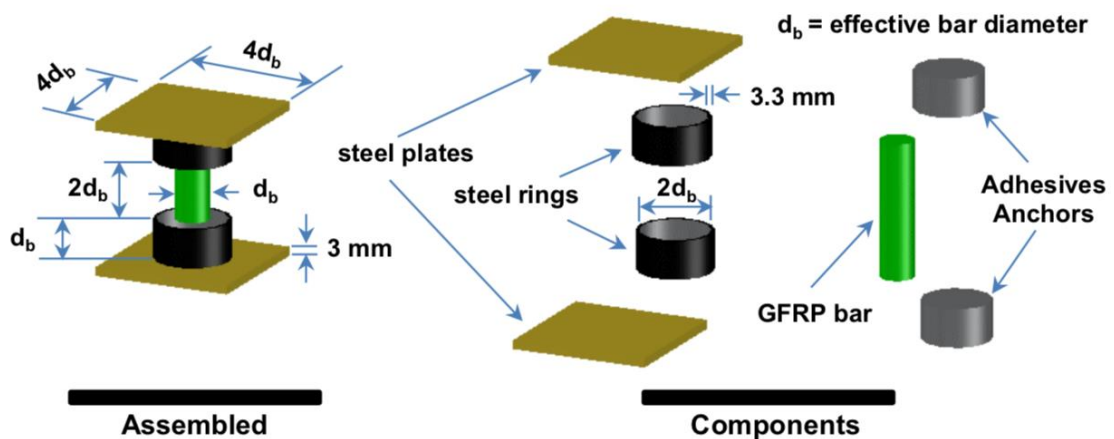


Figure 2.2: Sample test setup by Khorrarnian et al. [32]

Tests were also conducted by Khorrarnian et al. [33] to evaluate the compressive elastic modulus and strength. The compressive properties of the rebars were examined by applying a pure-axial load on short GFRP bar specimens with an unsupported length equal to two times the diameter of the rebars. Two steel caps, including a steel hollow cylindrical section with an inner diameter of 32 mm (twice the length of the diameter)

and a depth of 12.7 mm, were used to remove the stress concentration at the ends of the rebar specimens. It was observed from the tests that the elastic modulus obtained from compression is close to that obtained in tension. The authors were uncertain whether the performance of GFRP bars under compression in concrete is the same as in the coupon test. They have concluded that it was too conservative not to include the GFRP contribution in compression and have suggested to consider the contribution of compression GFRP bars as linear elastic materials until concrete reaches its 0.003 mm/mm compressive cracking strain limit. Figure 2.3 shows the test setup.

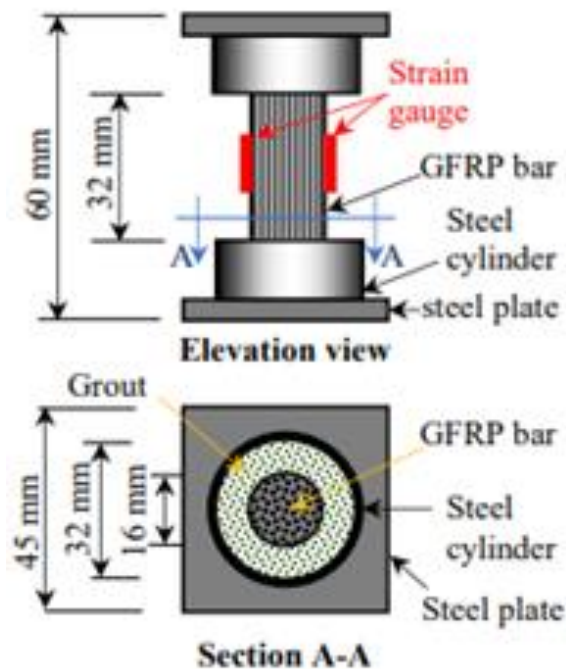


Figure 2.3: Sample test setup by Khorramian et al. [33]

Deitz et al. [34] investigated 15 mm diameter GFRP rebars of a length either less than 110 mm for no buckling or greater than 210 mm to check for buckling. A hole of 17 mm diameter was drilled in the threaded rod to allow 65 mm of the specimen inside, as illustrated in Figure 2.4. The hole size was bigger than the diameter of the rebar to allow some rotation. The authors found that for non-slender rebars, the ultimate compression strength ($f_{u,c}$) is equal to around 50% of the ultimate tensile strength ($f_{u,t}$). Also, based on restricted testing, it was found that the elastic modulus in compression ($E_{f,c}$) can be considered roughly equivalent to that in tension ($E_{f,t}$).

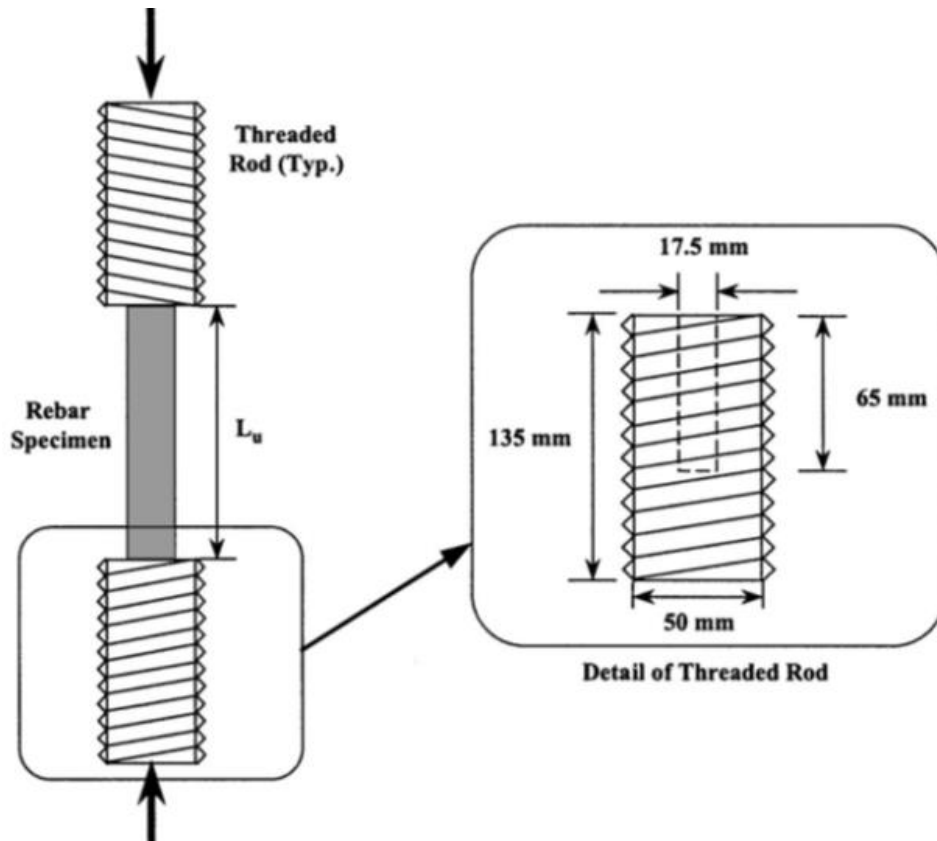


Figure 2.4: Sample test setup by Deitz et al. [34]

Additionally, a study by Khan et al. [35] examined the performance of 15 and 16 mm diameter CFRP bars of 60 and 80 mm lengths, respectively, under compression. Each test specimen, of smooth parallel ends, was placed vertically between the loading ends, as shown in Figure 2.5. A simplified ASTM D695-10 [36] compression test method for rigid plastics was conducted. The testing was done using 100 kN Instron UTM, and specimens were tested under a displacement-controlled rate of 1.0 to 1.3 mm per minute until failure. The modulus of elasticity in compression for CFRP bars was 1.17 times greater than that of GFRP bars. The modulus of elasticity in compression of GFRP bars (42.0 GPa) obtained was almost identical to the value (42.5 GPa) reported by Deitz et al. [34]. Also, the ultimate tensile strengths of CFRP and GFRP bars were 94% and 65% higher than their ultimate compressive strengths, respectively. Moreover, the compressive elastic modulus of CFRP and GFRP bars were 89% and 33% lower than their tensile elastic modulus, respectively.

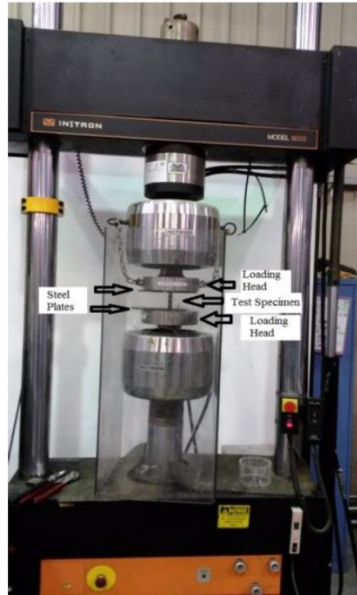


Figure 2.5: Sample test setup by Khan et al. [35]

Finally, a recent study by Thiyagarajan et al. [37] examined BFRP bars under compression, as shown in Figure 2.6. The specimen was mounted vertically between the compression testing machine's steel plates. The load was applied at a uniform rate until failure. The typical failure mode of the BFRP bars in compression was due to crushing of longitudinal fibers. It was found that the compressive strength is two times less than the tensile strength of the BFRP bars. It was also found that the ultimate compressive strength of the BFRP bars varies with the change in the diameter.



Figure 2.6: Sample test setup by Thiyagarajan et al. [37]

Table 2.2 summarizes the test results from the literature review available. The comparison includes the material type, the diameter of the sample, the unsupported sample length, the loading rate, and the strength and compressive modulus of elasticity with respect to the tensile properties. The results were not in agreement together to give a clear-cut conclusion on the compressive mechanical properties due to the different sample setups and material manufacturing quality.

Table 2.2: Compressive strength and elastic modulus of FRP bars as reported in previous studies

Source	Material	Diameter (mm)	Length (mm)	Loading rate	E value % of tension	Strength % of tension
Plevkov et al. [31]	GFRP/CFRP	10	50	-	67% / 73%	61% /53%
Khorrarnian et al. [32]	GFRP	13/16/19	4 times the diameter (2 times for the free length)	0.5mm/min	102% to 109%	66% to 85%
Khorrarnian and Sadeghian [33]	GFRP	16	32	-	122%	106%
Deitz et al.[34]	GFRP	15	110 for no buckling 210 for buckling	-	100%	50%
Khan et al. [35]	CFRP/GFRP	15/15.9	60/80	1to1.3mm/min	33% /89%	65% /94%
Thiyagarajan et al. [37]	BFRP	8/10/2012	2 times the diameter	-	39%, 42.4% /44.8%	35%

2.2.3. Effect of varying loading rate and type on FRP bars under compression. Varying the strain rate will change the results of the strength and strain properties [31]. The effect of strain rate on the tensile properties of GFRP composites was studied by Rotem and Lifshitz [38] and found that the dynamic strength is three times the static strength value, while the dynamic modulus is 50 percent higher than the static modulus value. On the other hand, while investigating GFRP composites, Rotem

and Lifshitz [38] found that the modulus of elasticity was not affected by the strain rate and the dynamic failure stress was only slightly more than the static value.

The automatic control system allows one to perform axial strain-controlled or axial stress-controlled tests. Then, strain-controlled and stress-controlled testing are deployed to plot a stress-strain curve. Theoretically, both approaches should yield the same results. In the samples where the material characteristics will yield and reach the plastic zone at a certain stress value, strain controlled testing will produce accurate results while stress-controlled testing will not produce accurate results because there will be a range wherein the strain increases at a constant stress value. However, FRP materials do not yield, and thus, using stress-controlled testing is accurate. The main advantage of stress-controlled testing is that it is a closer representation of the behavior elements undergo in existing structures. Abed et al. [39] performed a series of static and dynamic compressive tests on different FRP bars. They have reached to a conclusion that few FRP bars exhibited different variation in their compressive strengths at high loading rates.

For strain-controlled testing, the test is conducted such that the sample will be tested at a given strain rate. Generally, the specimen is tested at a uniform strain rate. With a known strain rate, a stress-strain rate curve can be plotted.

2.2.4. Challenges and observation on concrete columns reinforced with FRP bars. Because of the discrepancies in the investigated ultimate compressive strength and compressive modulus of elasticity of the FRP bars and their contribution as main reinforcement in concrete columns, there is still no theoretical equation recommended in CAN/CSA S806-12 [40] or in ACI 440.1R-15 [7] to estimate the maximum axial capacity of FRP-RC columns to carry loads. However, several theoretical equations to estimate the maximum axial load carrying capacity of FRP-RC columns have been proposed in previous studies. Nevertheless, these equations have not been sufficiently assessed using an extensive range of experimental data [41].

The predominant elastic behavior of FRP rebars usually results in minimal warning before a brittle and sudden failure occurs. Thus, satisfying deflection and ductility design requirements is a challenge when designing FRP reinforced concrete structures [42]. The FRP-concrete bond can be enhanced by means of mechanical

anchorages such as sand coating and surface deformations. Nevertheless, the lower ductility of FRP rebars will remain a major concern, especially in structures subjected to dynamic loading [42]. To estimate the mechanical behavior of FRP bars as internal reinforcement for RC structures, additional analyses should be performed since the change in the material properties, technological factors and external aspects may change the general structural performance of newly-developed bars [43].

A study by Prachasaree et al. [44] evaluated experimentally the structural performance and behavior of GFRP-RC columns under axial compression loading. Specimens were prepared with various longitudinal reinforcement, transverse reinforcement and concrete cover. In accordance to this study, the ratio of GFRP longitudinal and transverse reinforcement slightly affected the columns' strengths. Although there was little variation in strength between various types of transverse reinforcement, the spiral lateral reinforcement was noticed to be the most influential factor among other factors, such as inelastic deformation and confining pressure. The effect of the transverse reinforcement on deformability is more prominent than that on the column strength. Increasing the reinforcement ratio of GFRP increased the contribution to the confined compressive strength. The concrete cover did not affect the maximum load strength or late stage deformation, but rather predominantly affected early confinement effects.

2.2.4.1 Concentrically-loaded short columns reinforced with FRP. The majority of the studies performed on concentrically-loaded short columns reinforced with FRP focused at measuring the amount of contribution of the main FRP reinforcement bars to estimate the ultimate capacities of the tested columns. The contribution of FRP bars in the columns' ultimate capacity depends on the type of the FRP bars used due to the different mechanical properties that they possess. Table 2.1 briefly summarize the properties of GFRP and BFRP bars and compares them with different well-known construction materials. Comparing FRP bars with steel bars in terms of contribution was the main concentration of numerous studies, since steel is one of the mostly used construction material. Several studies such as Tobbi et al. [45], Afifi et al. [46] and Pantelides et al. [47] has studied the contribution of FRP bars in short concentric columns and came up with proposed equations. ElMessalami et al. [30] gathered and analyzed the outcome of hundreds of tests published in over 40 different

experimental and analytical studies. The gathered columns were categorized in accordance to their loading regime, slenderness, concrete type, cross sections, and reinforcement material and ratio. The design equations suggested by numerous authors were gathered and evaluated to estimate the load-carrying capacities of the columns tested.

2.2.5. Challenges and observation on finite element modeling of columns reinforced with FRP. A section analysis with the assumption that “plane sections remain planar before and after loading” is frequently implemented to analyze the ultimate strength and various load-deformation relations of beams and columns [48], [49].

The main bar's reinforcement in ABAQUS are modelled as embedded elements, which is a technique used to describe an element that lies embedded in a group of host elements (concrete) whose response will be used to constrain the translational degrees of freedom and pore pressure degree of freedom of the embedded nodes. The embedded element can either be chosen to be truss-in-solid or solid-in-solid, and this decision is left for the researcher to specify.

Elchalakani et al. [50] designed the geometry of the FE models in Figure 2.7 according to drawings shown in Figure 2.8. The concrete was modelled as a homogenous three-dimensional solid element. The longitudinal and transverse reinforcement were modelled as three-dimensional wire elements. With a diameter of 14 mm each and a length of 1.17 m, the six longitudinal bars were described. With a bar diameter of 10 mm, the ligatures were specified and engineered so that they had a 27.5 mm cover. The behavior of the elastic-plastic behavior of concrete was modelled in accordance to the well-known damage plasticity model by Liu et al.[51]. GFRP bars and stirrups were simulated without damage criteria with linear elastic material up to failure. In ABAQUS, the GFRP bars and stirrups were embedded in the concrete sections. Therefore, there was no simulation of the interface between the concrete and GFRP bars. The two materials were regulated by material models of their own. The ABAQUS built-in constraint "embedment" was used to model the interaction between the reinforcement and the concrete. Based on the confinement model by Kappos and Konstantinidis [52], the concentric columns were partitioned to segregate the regions of unconfined and confined concrete. The stress distributions for the OPC concrete

specimens were identical to the GPC specimens. The models obtained an average difference of 8 percent in peak load between the experimental and FE predictions and 11 percent in deflection at peak load for the OPC concrete specimens. However, the models appeared to overestimate the maximum load, which is particularly seen for the columns loaded concentrically. The overestimation occurred only with the eccentrically loaded column with 75 mm stirrup spacing. For the OPC concrete beam O150-F with a 15 percent deviation from the experimental outcome, the greatest inaccuracy in the simulation occurred, indicating the premature failure caused by lapped stirrup opening. The broad difference between the FE-predicted displacement and the experimental results also resulted from this.

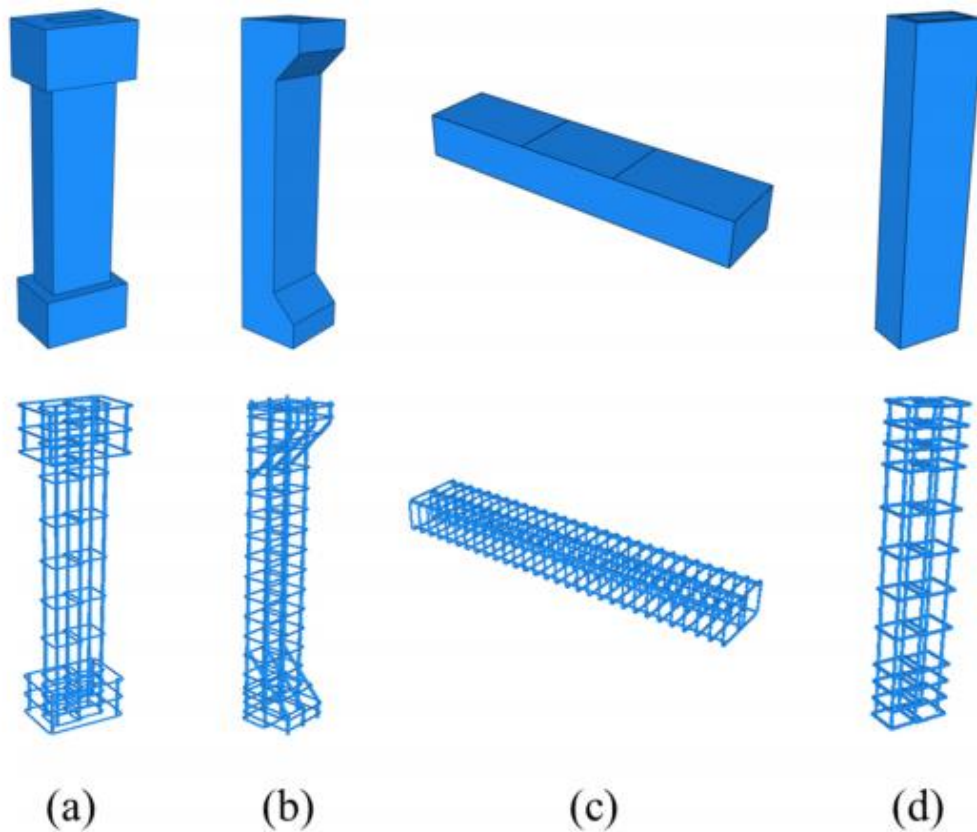


Figure 2.7: The typical geometry by Elchalakani of the FE models of, (a) concentrically loaded columns, (b) eccentrically loaded columns, (c) GPC and OPC concrete beams (d), OPC concrete columns [50].

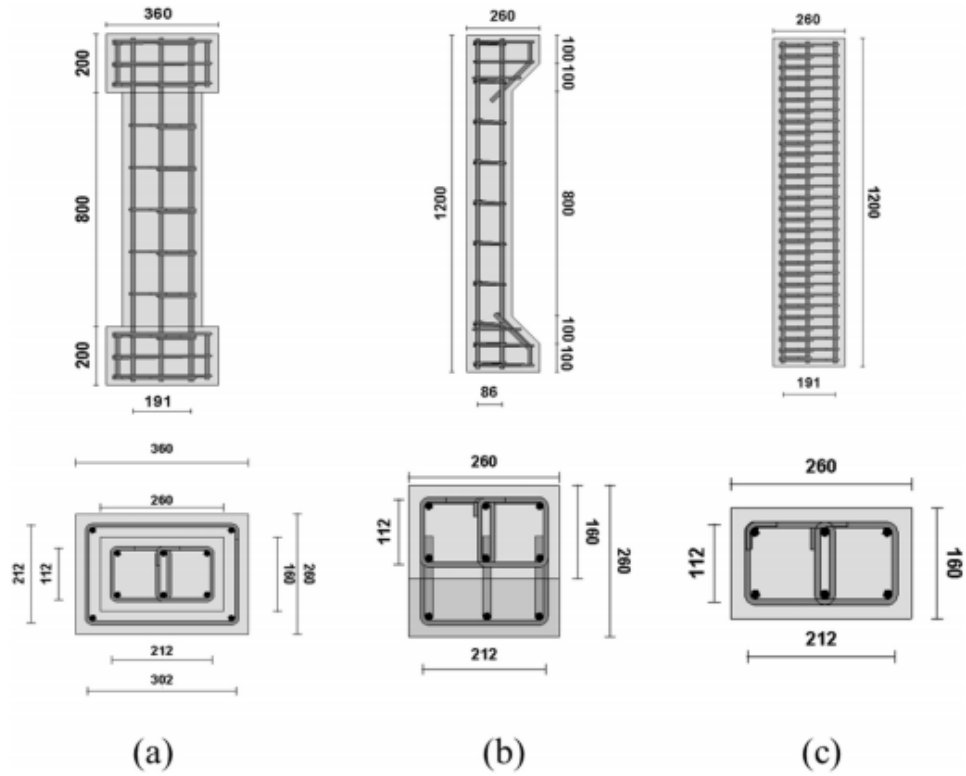


Figure 2.8: Sketch of RC columns by Elchalakani, (a) concentrically loaded column, (b) eccentrically loaded column, (c) beam. (in mm) [50].

It was found that it is possible to use an available confinement model to reliably simulate the concrete specimens' behaviors in elastic and plastic zones of different types of concrete. It was shown that by selecting the concrete damage plasticity (CDP) model the experimental load-deflection diagrams were closely estimated. For both types of concrete specimens, maximum load and deflection at maximum load have been well predicted at a reasonable degree of precision (on average 14 percent and 11 percent for GPC specimens and 8 percent and 11 percent for OPC concrete specimens, respectively). The typical FE results are shown in Figure 2.9 Due to the opening of the lapped stirrups, the discrepancies primarily came from premature failures. To avoid such an unfavorable failure mode, it is advised to assemble the specimens using stirrups with a spacing being at least 50 percent of the perimeter length. It is concluded that GPC sample models implementing the theory of CDP and the GFRP bar stress-strain response approach would be appropriate for accurately simulating the behaviors of GPC columns and beams with sufficiently strong stirrups and creating safe designs.

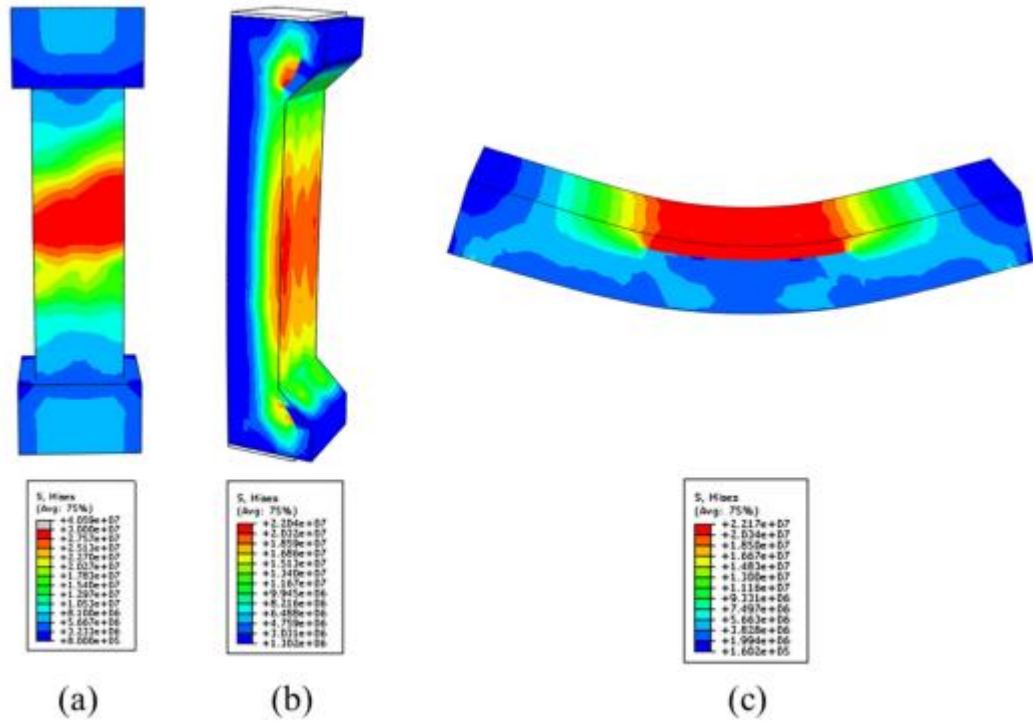


Figure 2.9: Typical FEA results for (a) concentrically loaded columns, (b) eccentrically loaded columns, (c) RC beams [50].

Another study by Abed et al. [53], where they studied the axial behavior of short circular RC columns reinforced with GFRP bars and spirals, and short square RC columns reinforced with BFRP bars experimentally and numerically. To predict the axial behavior of RC columns under concentric and eccentric loading, nonlinear finite element models were developed. Several parameters such as GFRP ratios of main and transverse reinforcement were investigated and an interaction diagram was developed for RC columns. ABAQUS software was used to model the nonlinear finite element model of both GFRP-RC and BFRP-RC. The used materials were tested in the experimental program and their properties were incorporated into the finite element model developed. The nonlinear behavior of the concrete material was modelled by introducing the actual inelastic properties of the concrete in the model. The concrete plasticity parameters were defined with 36 dilation angle, 0.1 eccentricity, 1.16 of f_{b0} biaxial compressive strength of concrete over f_{c0} uniaxial compressive strength of concrete, 0.667 of shape of yield surface parameter and a viscosity of 1×10^{-5} . Additionally, to account for large deformation, the nonlinear analysis (NLGEOM)

option was activated in the model used. On the columns, several load-eccentricities were applied and the load-displacement graphs for all eccentricities applied were retrieved. From the FE analysis, the load versus axial strain graphs were obtained. Under the influence of the longitudinal reinforcement ratios, the modeling of RC columns reinforced with GFRP bars was carried out by varying the number of longitudinal bars while maintaining the same diameter. The authors found that the numerical results of the axial behavior of columns reinforced with FRPs were in lined with the experimental results. Abed et al. also reported that increasing the reinforcement ratio of the column would increase the axial capacity as well as the ductility of the column. The capacity and ductility also increased as the spiral area increased, while maintaining the pitch at a value in which confinement occurs. When the pitch of the spirals decreased, the maximum load and ductility increased since confinement is better.

2.2.6. Evaluation of the mechanical properties of concrete. Concrete is a very old material. Cement was used in ancient times in Egypt, Greece, and Rome. The word "cement" comes from a Latin word referring to a solid material to which water has been added [54]. In 1824, Joseph Aspdin invented the name "portland cement," and thus changed the way modern infrastructure would be constructed to the present day [55]. Since extensive and reliable information is available about the mechanical properties of concrete, the properties were obtained from the literature review.

2.2.7. Failure mechanisms of concrete under different loading rates. The rate dependency of concrete can be divided into two regimes: the regime with moderate rate effects for loading rates in the range from 10^{-4} GPa/s (static) up to 50×10^{-4} GPa/s, and the regime with extensive rate effects for loading rates beyond 50×10^{-4} GPa/s. It is assumed that the moisture content plays an important role in the increase in concrete strength. Crack branching and bridging occur under static loading conditions. Cracks have more time to grow in the weakest spots due to the low loading rate and thus form around the aggregate particles. When the loading rate is very high, cracks have less time to form, and are thus not limited to the weakest spots in the cement mixture, the transition zone. Hence, cracks do not only occur around the aggregate particles, but also within them. A set of results and conclusions have been taken from a study by Vegt et al. [56] where the failure mechanisms in concrete under static loading is studied using

the Split Hopkinson Bar (SHB), which is used to generate moderate loading rates, and the Modified Split Hopkinson Bar (MSHB), which is used to generate high loading rates. The static and the SHB fracture mechanisms are similar, except for the crack bridging process in the static tests, which makes the failure behavior more ductile than in the SHB tests. The MSHB's failure is dominated by the presence of several micro-cracks that spread, evolving into one or more macro-cracks. In this high loading rate regime, energy dissipation is very high and is dominated by fractures at the micro-scale rather than at the macro-scale. For the MSHB-test condition, the stress strain relation originated from the fresh experimental data is affected by the inertia effects in the structural response, resulting in higher values for the fracture energy [56].

2.2.8. Design equations for FRP-RC columns. Numerous studies have examined the behavior of rectangular and circular columns reinforced with glass FRP and stirrups, and have suggested equations to estimate the ultimate concrete capacity reinforced with FRP main bars in compression. Table 2.3 shows several equations to predict the axial ultimate capacities of FRP-RC columns.

Table 2.3: Summary of the design equations presented in the literature for FRP-RC columns

Reference	Suggested equation	Equation
A- Neglecting the contribution of FRP		
CSA S806-12 [57]	$P_o = \alpha_1 f'_c (A_g - A_F)$	(2. 1).
	$\alpha_1 = 0.85 - 0.0015 f'_c \geq 0.67$	
ACI 318 [58]	$P_o = 0.85 f'_c (A_g - A_F)$	(2. 2).
B- Considering the FRP contribution		
Afifi et al. [46]	$P_o = 0.85 f'_c (A_g - A_F) + \alpha_g f_{fu} A_F$	(2. 3).
	$\alpha_g = 0.35$	
Pantelides et al. [47]	$P_o = 0.85 f'_{cc} A_c + 0.0035 A_{FRP} E_{FRP}$	(2. 4).
	$f'_{cc} = f'_c + \varphi_f 3.3 f_{1FRP}$	

$$f_{1FRP} = \frac{2E_{FRP}A_{spFRP}\varepsilon_{fe}}{sd_c}$$

$$\varepsilon_{fe} = k_e\varepsilon_{fu}$$

$$(\varphi_f = 0.95, k_e = 0.55)$$

$$\text{Tobbi et al. [45]} \quad P_o = 0.85f'_c(A_g - A_F) + \varepsilon_{co}\alpha A_{FRP}E_{FRP} \quad (2. 5).$$

A_c = area of confined concrete core; A_F = area of FRP longitudinal reinforcement; A_g = area of gross column section; f'_c = compressive strength of concrete; f'_{cc} = compressive strength of confined concrete; α = reduction factor; ε_{fu} = ultimate FRP strain; A_{spFRP} = area of FRP spiral; d_c = outside diameter of spiral; s = spiral pitch., ε_{co} = concrete strain at peak stress

The suggested equations are also listed in Table 2.3 Though some researchers recommended ignoring the contribution of the longitudinal FRP bars to the columns' capacities as listed in "A- Neglecting the contribution of FRP", other researchers adopted several approaches to determine such contribution as listed in "B- Considering the FRP contribution". The next sections discuss the several methods that researchers have followed to compute the contribution of FRP bars to the ultimate capacities of FRP-RC columns.

2.2.8.1. Neglecting the contribution of FRP bars in compression. New codes are allowing the use of FRP bars under compression. Yet, the design guideline ACI-440.1R-15 [59] prohibits using FRP bars as reinforcement in compression members. According to CSA-S806 [57] , the nominal unconfined axial load capacity of columns with FRP longitudinal reinforcement is determined in accordance with Equation 2. 1 (Table 2.3), in which the contribution of FRP bars to the columns' capacities is not considered. Ignoring the contribution of FRP bars to the capacities of FRP-RC columns underestimated the columns capacities averagely by 20% and 13% for equations 2. 1 and 2. 2 respectively for all groups that are confined with steel lateral reinforcement. This approach underestimates the capacity of FRP reinforced columns. Hence, the contribution of FRP rebars should be accounted for to a certain extent, in order to truly determine the actual capacity of FRP reinforced columns.

2.2.8.2. Considering the contribution of FRP bars in compression. Several researchers have chosen to consider the contribution of FRP bars by applying a

reduction factor to account for the low compressive strengths of FRP bars. Equation 2. 2 by Afifi et al. [46] considers the concrete compressive contribution plus to a reduced contribution from the FRP bars, as shown in Table 2.3.

Other researchers have chosen to account for the contribution of FRP bars by using the strength of FRP bars at certain level of FRP strain.

Pantelides et al. [47] proposed Equation 2. 4 (Table 2.3), which considers the strength of confined concrete core, f'_{cc} , while forecasting the capacities of FRP-RC columns to reflect the spalling of concrete cover observed at failure. In their equation, Tobbi et al. [45] used ε_f equivalent to the concrete strain limit, ε_{co} Equation 2. 5 in Table 2.3.

Chapter 3. Experimental Evaluation of BFRP and GFRP Bars under Compression

This chapter presents a detailed step by step explanation of the description of the GFRP and BFRP bars test material, the description of the specimen design and preparation in evaluating the compressive strength of commercially produced $\phi 8$, $\phi 12$, and $\phi 16$ GFRP and BFRP bars, description of the test matrix, an outline of the sample testing procedure, the instrumentation used in the tests, and the experimental results.

3.1. Test Material

The GFRP and BFRP bars were produced by Galen, a Russian company based in the city of Cheboksary. The GFRP and BFRP bars were manufactured by pultrusion, in which the fibers (glass or basalt) are impregnated with polymer binder, and then run through the system drain bushing. Figure 3.1 shows samples of the BFRP and GFRP bar specimens prepared for the compression test.

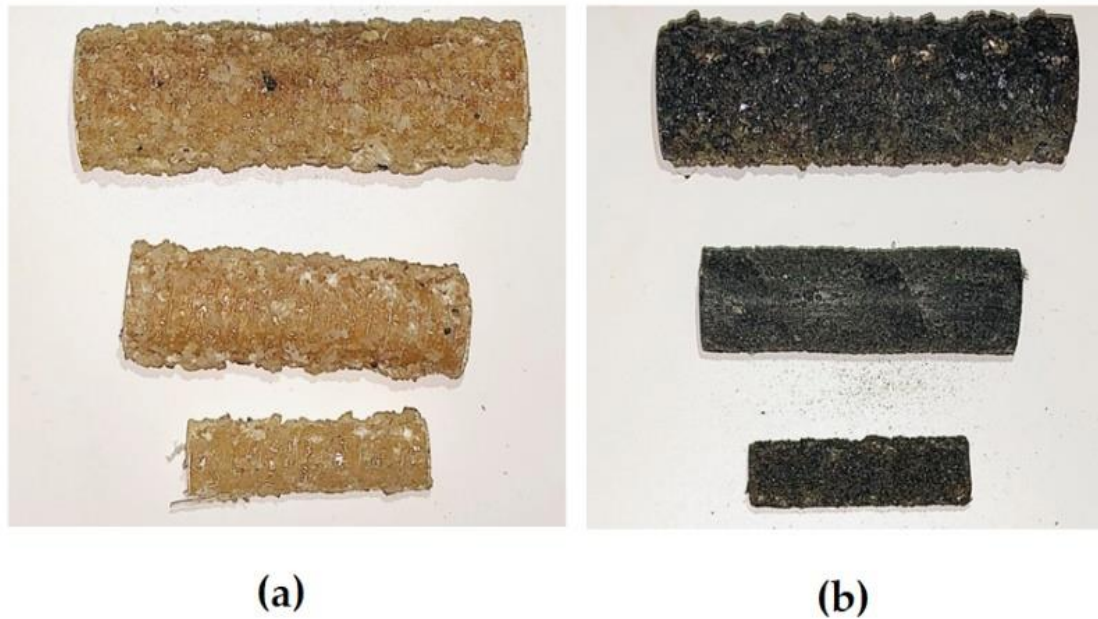


Figure 3.1: FRP bars samples (a) GFRP bar samples (b) BFRP bar samples

The properties of these bars in tension are shown in Table 3.1 were obtained by researchers in previous studies [17], [39], [60].

Table 3.1: Tensile properties of bars reinforcements [17], [39]

Sample Material	Sample Diameter (mm)	Ultimate Tensile Stress (MPa)	Tensile Modulus of Elasticity (GPa)
GFRP	8	983.1 ± 32	
GFRP	12	976±46	
GFRP	16	874±39	44.9±1.3
BFRP	8	1075.1 ± 37	
BFRP	12	1118.6 ± 31	
BFRP	16	1121.3 ± 56	49.3±1.1

3.2. Specimen Design and Preparation

In order to get accurate results on the compressive strength of the GFRP and BFRP bars, it must be ensured that the loading on the bars during testing is purely concentric. In addition to that, the effective length of the bars must not be too long and hence cause buckling. GFRP and BFRP bar specimens were manufactured by a cutting machine in which bar ends were ensured to be smooth and level. As discussed in the literature review, when the bar specimens have a length less than three times their diameter, buckling will not occur. As such, the bars are cut into lengths two times and three times their diameters. Three types of apparatus were made, and the third testing apparatus was used. The FRP bars will be fabricated such that the inner diameter of the steel tubes was 1-1.5mm higher than the diameter of the bar sample. The bars were placed inside steel grips from both ends. It was difficult to obtain a perfectly flat end perpendicular to the loading axis with the equipment available.

3.3. Test Matrix

A total number of 30 GFRP and BFRP bars were tested under compressive axial loading to study their compressive mechanical properties. The bars are identified and named systematically based on the material of the bars, their diameter, and their total length. The first part indicates the material of the bars (GFRP or BFRP). The second part indicates the diameter of the bars. The third part provides information about the length of the bars. For example, G12-24 means that the bar is a GFRP bar, has a diameter of 12 mm, and has a length of 24 mm. Table 3.2 shows the specimen matrix

used in this study. Five samples were tested for each bar ID, and the average and standard deviations of the results of each bar ID were recorded.

The results are compared to the tensile values calculated in previous experiments. The comparison will provide a generalized behavior of the bars in compression to their behavior in tension. Table 3.2 shows the proposed text matrix for GFRP and BFRP bars under compression.

Table 3.2: Test matrix

Bar ID	Diameter (mm)	Sample length (mm)
G8-16	8	16
G12-24	12	24
G16-32	16	32
B8-16	8	16
B12-24	12	24
B16-32	16	32

3.4. Test Setup and Procedure and Instrumentation Used in the Tests

Two test setups were attempted before deciding on the final test setup. The first test setup included a steel tube welded to a plate. The bar was placed inside the tube and an epoxy was added to prevent the bar from tilting while testing. Figure 3.2 and Figure 3.3 show the first arrangement.

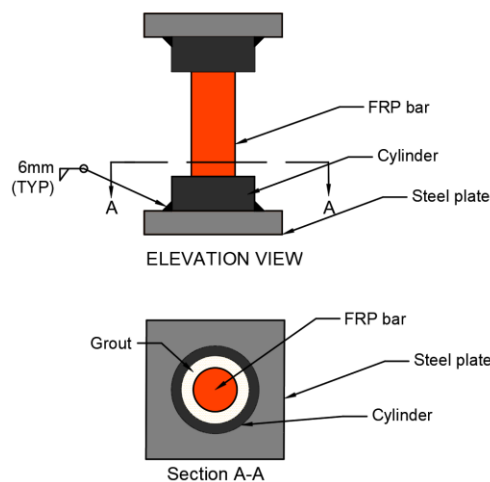


Figure 3.2: First attempted test setup sketch

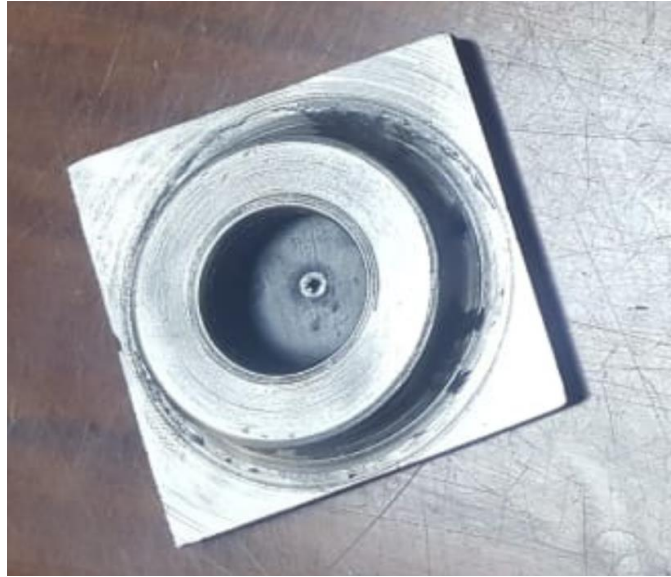


Figure 3.3: First attempted test setup typical one end

Although the approach of testing the bars by this setup achieved the desired intent, two major difficulties were encountered which induced undesired eccentricity and resulted in a tilted bar setup and inaccurate results. The first difficulty was placing the bar in the middle of the cylinder; even though a mark was drawn on the centroid of the plate by the fabricator, placing the bar manually in the middle was difficult. The second difficulty was that the steel plate and cylinder were relatively heavy to the arrangement, therefore, when placing the second end of the bar into the other plate, the first arrangement was ruined, and the bar shifted away from the center. This resulted in immature failure of samples.

A second setup was then attempted. This setup included an open tube filled with epoxy, with the FRP bar being placed inside the epoxy. The proposed arrangement in Figure 3.4 and Figure 3.5 was chosen to try to avoid stress concentration at the end of the bar specimens by using the steel grips. Placing the bar at both ends was done with a tool that keeps the bar and the end steel grips placed at a 90 degrees angle. Figure 3.5 shows the tool and the way the bars were handled. GFRP and BFRP bars were placed in the desired opening and then an epoxy was applied to the steel grip. Afterwards, the alignment arrangement was removed before testing.

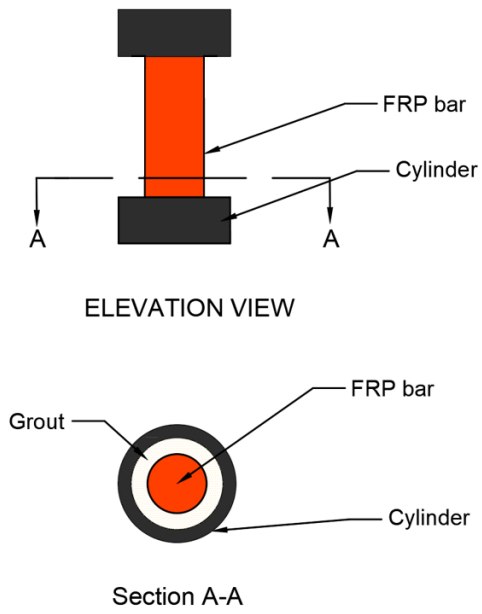


Figure 3.4: Second attempted setup schematic sketch



(a)



(b)

Figure 3.5: Second attempted test setup (a) alignment Tool (b) sample specimens

After conducting the test for the first attempted test setup, and checking the results and the samples failure mode, it was found that the load at failure was much lower than expected and the bars encountered premature failure which started from both ends of the bars. Handling the bars was the main issue; when the bars were placed at one end, the epoxy had to dry before the other end was fixed, and since the plate and the ring are relatively heavy, a small amount of tilting was hard to avoid, which caused an eccentricity of the loading and lead to premature failure.

The second attempted test setup resulted in premature failure modes of the FRP bars as well. The alignment tool did indeed place the bars at the middle of the grip and made them completely perpendicular. The alignment tool was placed after applying the epoxy, and after removing this tool, the epoxy would have bonded to the tool. Therefore, when the alignment tool was removed, the bars tilted, which made it extremely difficult to get a completely perpendicular sample.

The typical failure mode from the first two attempted setups is shown in Figure 3.6.

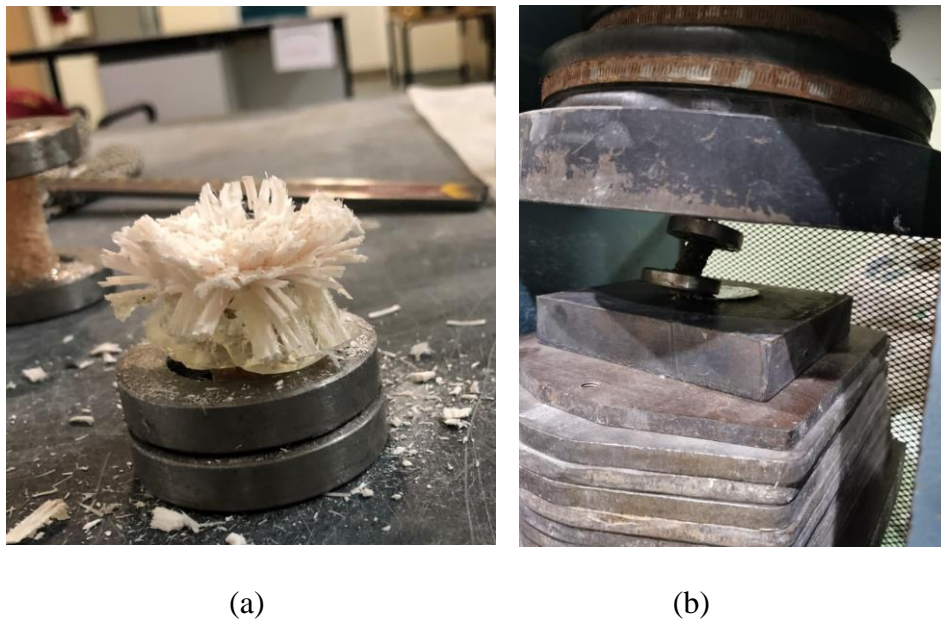


Figure 3.6: Typical attempted setups 1 and 2 testing outcome (a) typical sample failure (b) typical tilting of samples during testing

Finally, after two unsuccessful test setups attempts, a third test setup was adopted as shown in Figure 3.7 and Figure 3.8.

The length of each FRP bar specimen was two times the diameter, which is less than three times of its diameter so that the FRP bars do not buckle. Slightly oversized holes in the ends of the testing apparatus allowed some rotation at the ends of the specimens, thereby reducing the moments applied by the apparatus while still providing some end restraint.

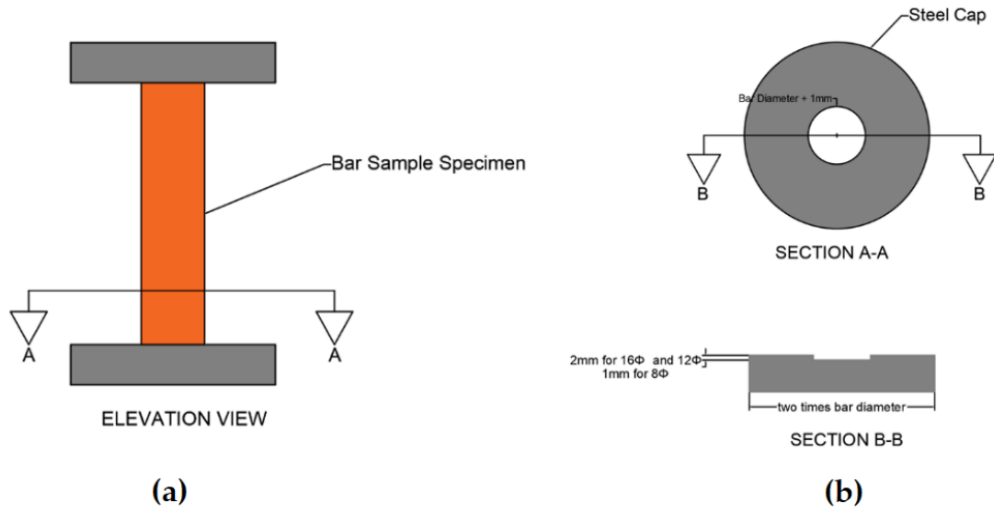


Figure 3.7: Used test setup sketch

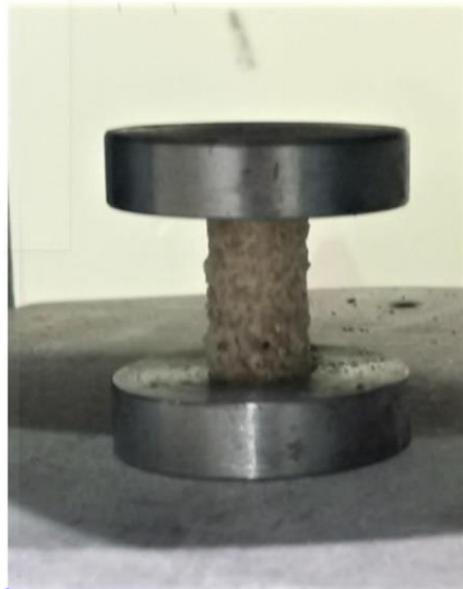


Figure 3.8: Used test setup

The compression tests were conducted at a rate of 0.25–0.5 MPa/s using a universal testing machine (UTM) with a capacity of 3000kN under compression as shown in Figure 3.9.

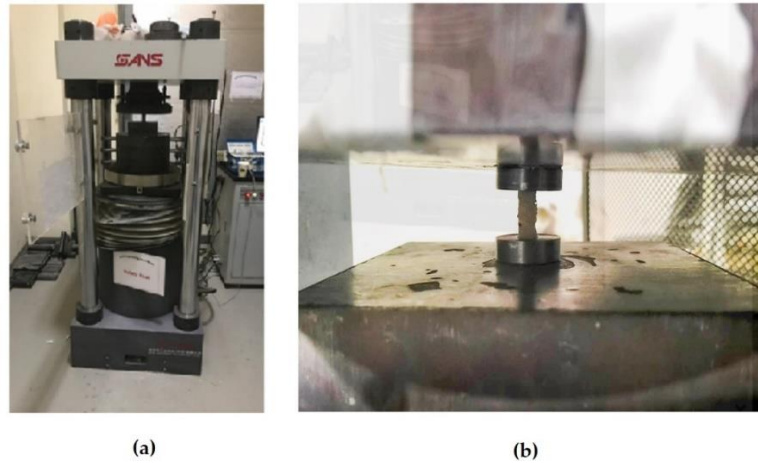


Figure 3.9: Experimental setup of static loading (a) an overview picture of the testing machine with the bar (b) a focused picture on the bar inside the testing machine

A cutting machine was used to ensure that the bar ends are completely perpendicular to the fixed surface. Cutting and shaping was performed by a rotating part clamped in a chuck. The bars held on a turret. Figure 3.10 shows the cutting apparatus.



Figure 3.10: Apparatus used for cutting the samples

3.5. Experimental Results

3.5.1. Compressive strength of bars and failure modes. Five bar specimens of each size were tested, and the average compressive strength and their standard deviations were reported, as shown in Table 3.3 and Table 3.4 for the GFRP and BFRP bars, respectively.

Table 3.3: Properties of GFRP reinforcements

Bar Diameter	Cross-sectional Area (mm ²)	Compressive Strength (MPa)	Average Compressive Strength (MPa)	Standard Deviation (MPa)
16.7	219	573		
16.7	219	544.2		
16.7	219	551.5	562.5	23
16.7	219	545.6		
16.7	219	598.1		
12.7	126.7	504.4		
12.7	126.7	480.8		
12.7	126.7	510.7	496.1	18
12.7	126.7	472.9		
12.7	126.7	511.5		
8	50.5	354.3		
8	50.5	294.9		
8	50.5	287	311.6	27.3
8	50.5	322.7		
8	50.5	298.9		

Table 3.4: Properties of BFRP reinforcements

Bar Diameter	Cross-sectional Area (mm ²)	Compressive Strength (MPa)	Average Compressive Strength (MPa)	Standard Deviation (MPa)
16.7	219	420		
16.7	219	471.9		
16.7	219	440.8	448.2	24.3
16.7	219	454.2		
16.7	219	441.8		
12.5	122.7	418		
12.5	122.7	430.3		
12.5	122.7	390.3	416.6	19.5
12.5	122.7	405		

12.5	122.7	439.2		
8.4	55.4	420.4		
8.4	55.4	416.8		
8.4	55.4	362.7	394.5	24.1
8.4	55.4	386.2		
8.4	55.4	386.2		

In general, the variation in the compressive strength results between the five specimens were reasonable for all sizes. However, and unlike their tensile strengths, the compressive strengths of both the GFRP and BFRP reported lower values at smaller sizes. In particular, the compressive strength of the 8 mm GFRP and BFRP bars were reduced by 45% and 12% as compared to 16 mm GFRP and BFRP bars, respectively. On the other hand, the compressive strengths of the BFRP bars were in the range of 35–41% of their tensile strengths. For the case of the GFRP bars, the compressive strengths of the 8, 12, and 16 mm bars were about 32, 51, and 64% of their tensile strengths. One noticeable failure mode was detected throughout the tests. It was a crushing failure mode in which the glass and basalt fibers separated from the resin matrix, as shown in Figure 3.11. The young's modulus in compression of both materials, on the other hand, was around 80% of that in tension.



(a)



(b)

Figure 3.11: Typical samples failure mode (a) GFRP sample (b) BFRP sample

Chapter 4. Evaluation of RC Columns Reinforced with GFRP and BFRP Bars

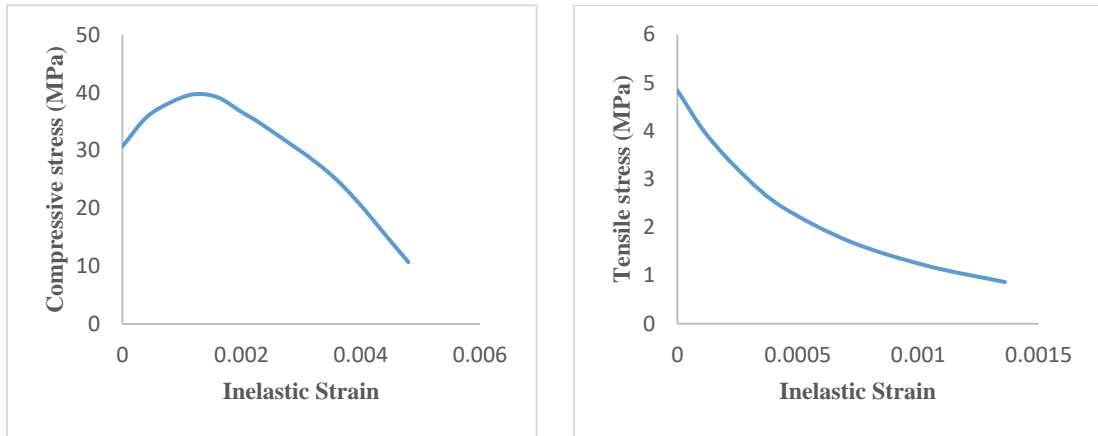
The axial behavior of the concrete columns reinforced with GFRP and BFRP bars is numerically investigated in this chapter. Nonlinear finite element (FE) models were developed to predict the axial behavior of the reinforced concrete (RC) columns under concentric and eccentric loading. Different parameters, such as the longitudinal reinforcement ratios, different cross sections, and transverse reinforcement material for the RC columns, were considered. The compressive and tensile properties of the GFRP and BFRP bars investigated in the previous section (Table 3.1, Table 3.3 and Table 3.4) were utilized in developing the FE model and in conducting the parametric analysis.

4.1. Finite Element Modeling

This section presents the development and verification of the FE models for concrete columns reinforced with GFRP bars (GFRP-RC columns) and BFRP bars (BFRP-RC columns). The commercial software package ABAQUS was used to create the nonlinear finite element models in which the axial behavior of the GFRP- and BFRP-RC columns were accurately simulated. The FE model verification was also performed using a set of experimental tests conducted previously by ElMesalami [61], [62] on similar columns.

4.1.1 Model material. The materials used in the models include GFRP, BFRP, steel and concrete. The concrete material was defined in the elastic zone through its elastic modulus and Poisson's ratio while the inelastic behavior is defined using the concrete damage plasticity (CDP) model. CDP approach, that guarantees the uniqueness and accuracy of the model. In which by this method, the input parameters obtained for a specific concrete class with a specific characteristic strength can be used for finite element simulation of the desired concrete. Utilizing the CDP approach allows defining both the compressive and tensile properties of the concrete material in the FE analysis. The CDP approach is designed specifically for the use of applications of materials such as concrete which is subjected to specific type of loadings such as monotonic or dynamic loading, and can be used for plain type concrete or concrete with rebar so user can define reinforcement.

Figure 4.1 illustrates the compressive and tensile properties for concrete used in the present FE analysis.



(a) (b)
 Figure 4.1: (a) Inelastic compressive and (b) tensile behaviors of concrete used in the FE Model.

For the CDP model, the plasticity parameters include the dilation angle of 36, eccentricity of 0.1, the ratio f_{b0}/f_{c0} of 1.16, the parameter K of 0.667 and viscosity parameter of 1.0×10^{-5} . The GFRP and BFRP materials are defined using the elastic modulus and ultimate strength. The GFRP and BFRP materials are defined using the elastic modulus and ultimate compressive and tensile strengths listed in Table 3.1, Table 3.3 and Table 3.4. The plastic behavior for the steel ties is defined using the yield strength for Grade 60 steel reinforcement (420 MPa).

The ultimate compressive strength was obtained from the test results, while Young's Modulus in compression was taken as around 80% of that in tension based on the experiments done earlier.

For the eccentric loading cases, the GFRP and BFRP bars subjected to tension will be given an elastic behavior with the strength characteristics of GFRP and BFRP in tension, and the GFRP and BFRP bars subjected to compression will be given an elastic behavior with strength characteristics of GFRP and BFRP in compression obtained from Table 3.1, Table 3.3 and Table 3.4.

4.1.2 Model geometry. The concrete column was modeled as a homogenous three-dimensional solid section using eight-node linear brick elements with reduced integration whereas the longitudinal and transverse reinforcements were modeled using deformable truss elements, which only carries axial load during bending. The transverse

reinforcements were defined with cross-sectional areas of 78.5 mm^2 and designed such that they were surrounded by a 27.5 mm concrete cover. Figure 4.2 displays the full model and the reinforcements along with the chosen mesh for the square cross-section of $180 \text{ mm} \times 180 \text{ mm} \times 1100 \text{ mm}$.

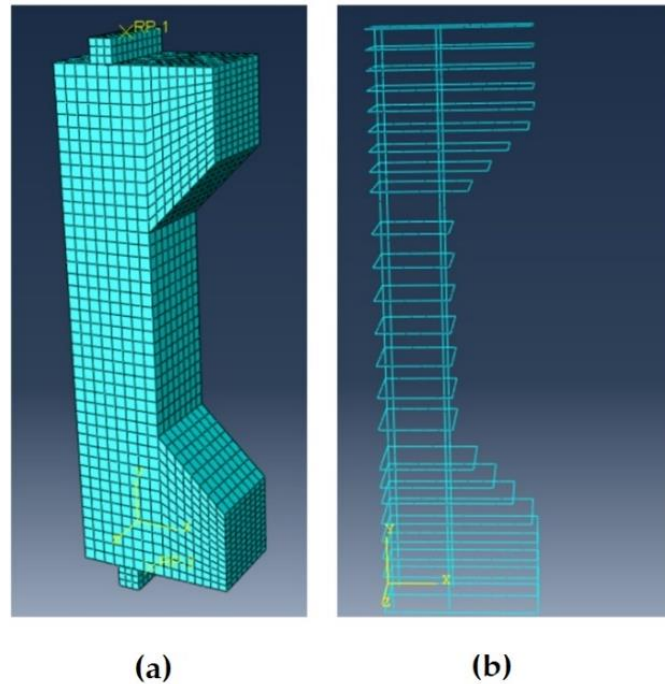
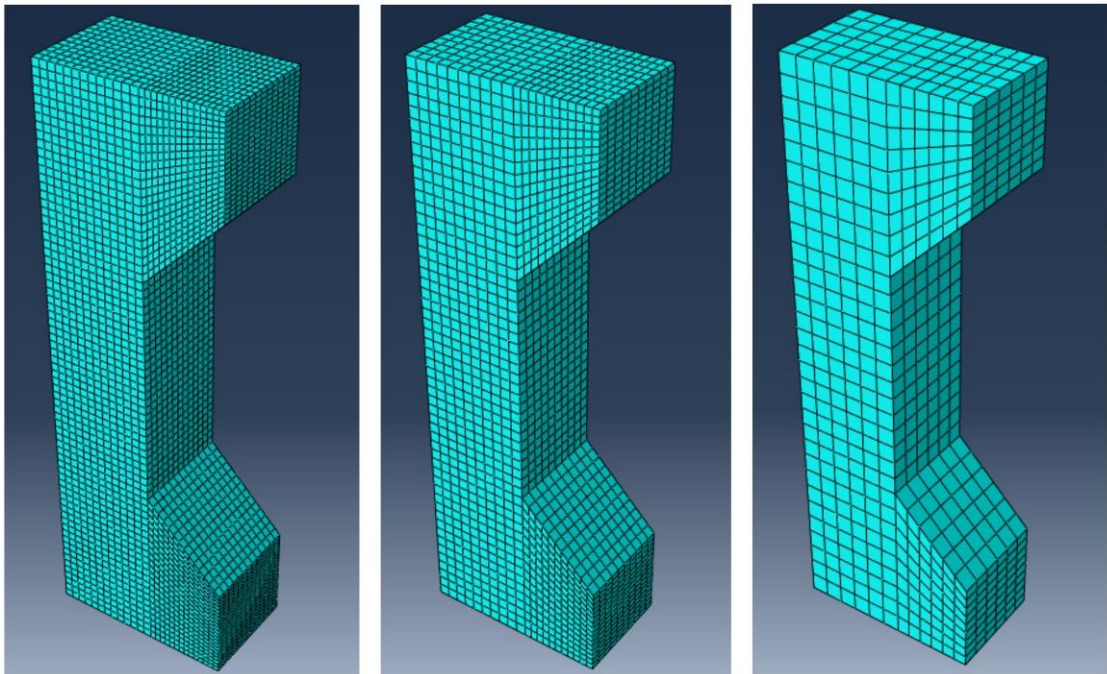


Figure 4.2: (a) Chosen mesh for the square cross section of (180x180x1100) mm (b) geometry of cage

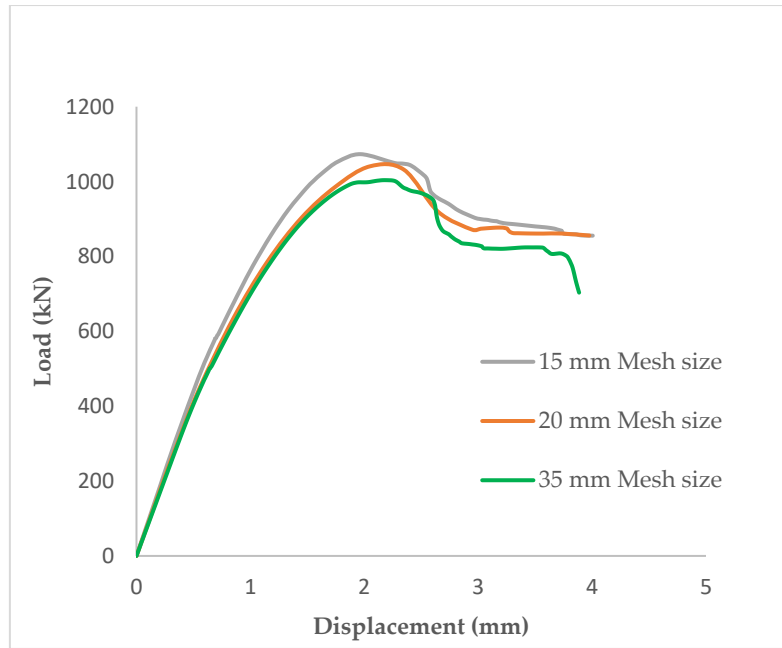
Three types of geometry were adopted in this study. Figure 4.2 shows the full model and the reinforcements along with the chosen mesh for the square cross section of $180 \times 180 \times 1100 \text{ mm}$. To simulate the interaction between the reinforcement and the concrete, the ABAQUS built-in constraint “embedment” was used. This constraint restricts the nodes of the reinforcement to the corresponding degrees of freedom of the host domain. As shown in Figure 4.2 (a), rigid plates were added to the model to ensure the uniformity of the load applied on the top and bottom surfaces. Moreover, normal and tangential surface-to-surface contact defined the interaction between the rigid plates and concrete surfaces using the penalty contact approach. Boundary conditions and displacement are assigned to the plates through reference points defined on the center of each rigid plate.

Static displacement-controlled loading is applied at the rigid plates to obtain the peak strength of the RC column. The column is restrained at the bottom along the horizontal and vertical components and also restrained from torsion. At the top, the column was restrained along the horizontal force component only. To model eccentricity in ABAQUS, a reference point at the desired eccentricity location must be first added before adding a rigid plate such that its centroid will be placed at the added reference point. In the opposite side of the column, a rigid plate was inserted in the centroid of the column. It shall be noted that a rigid plate is modelled such that failure shall not occur at that location. The eccentricity was changed by shifting the reference point and the rigid body to the required new eccentricity location.

A mesh sensitivity analysis was also conducted to select the appropriate mesh size that provide results accuracy with less computational cost. The model with a mesh size of 20 mm was considered through the analysis. The G16-0 model by ElMesalamani [61], [62] was chosen to perform a mesh sensitivity, in which it was found that reducing the mesh size will not affect the results, as shown in Figure 4.3.



(a)



(b)

Figure 4.3: (a) mesh configuration and (b) load vs. displacement results for the different element sizes.

4.1.3 FE model verification. The experimental program conducted by ElMessalami [61], [62] was partially to verify the FE modeling of rectangular concrete columns reinforced with GFRP and BFRP bars. The experimental program consisted of twenty-two reinforced concrete columns tested under monotonically increasing pure axial load. All columns were cast with normal-weight, ready-mixed concrete with an average compressive strength of 34.4 MPa. The verification results of only nine columns were presented.

Table 4.1 presents the details and axial capacity results for three selected column specimens.

Table 4.1: Test matrix, specimens' details and results [61], [62].

Column ID	Longitudinal Reinforcement		Eccentricity (mm)	Transverse Reinforcement		Pmax (kN)
	Type	Bar Diameter (mm)		Reinforcement Ratio (%)	Type	

S16-0	Steel	16	2.48	0	Steel	180	1300
B16-0	BFRP	16	2.48	0	Steel	180	1060
B16-40	BFRP	16	2.48	40	Steel	180	595
B16-80	BFRP	16	2.48	80	Steel	180	340
B20-0	BFRP	20	3.88	0	Steel	180	1070
B20-40	BFRP	20	3.88	40	Steel	180	750
G16-0	GFRP	16	2.48	0	Steel	180	1050
G16-40	GFRP	16	2.48	40	Steel	180	590
G16-80	GFRP	16	2.48	80	Steel	180	350

The column labels represent the reinforcement type and quantity, where the first letter refers to the longitudinal reinforcement type (B = basalt, G = glass, and S = steel). The first number after the letter refers to the diameter of the longitudinal reinforcement (16 or 20 mm) and the second number refers to the eccentricity value (0, 40, or 80 mm). Figure 4.4 and Figure 4.5 show the geometry and cross-sections detailing of the test specimens that were used in the FE model verification.

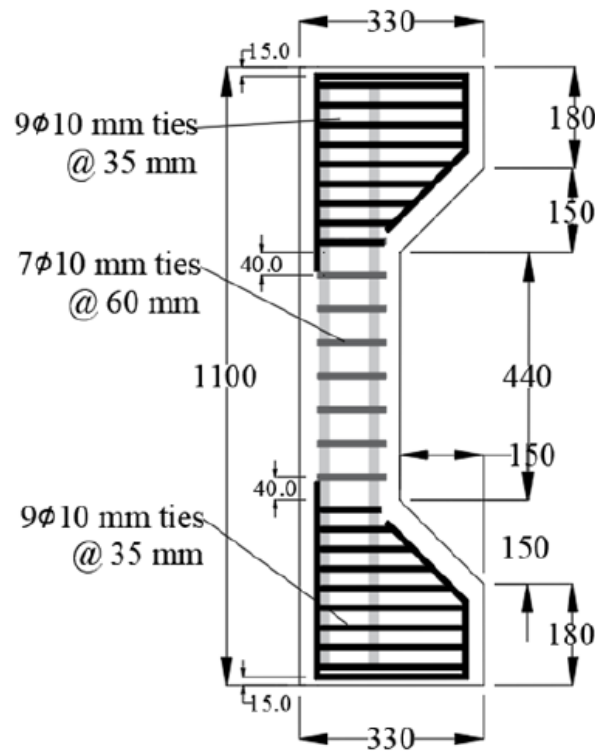


Figure 4.4: Experimental column by ElMesalami [61], [62].

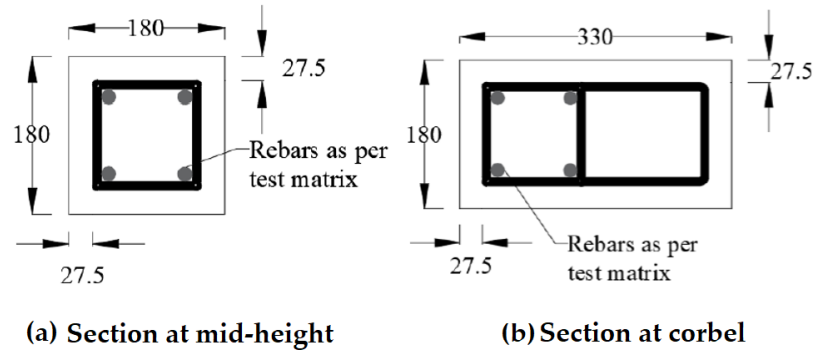


Figure 4.5: Columns cross section (in mm) by ElMesalami [61], [62].

Figure 4.6 and Figure 4.7 show the FE verification results as compared to the experimental data for the nine selected GFRP- and BFRP-RC columns.

The comparisons of the load vs. displacement curves (Figure 4.7) and the ultimate compressive strengths (Figure 4.6) between the FE model predictions and experiments were generally very good and within the approximate errors of 5%. Thus, the validated FE model was later used to conduct the FE parametric analysis for extending list of columns, as discussed next.

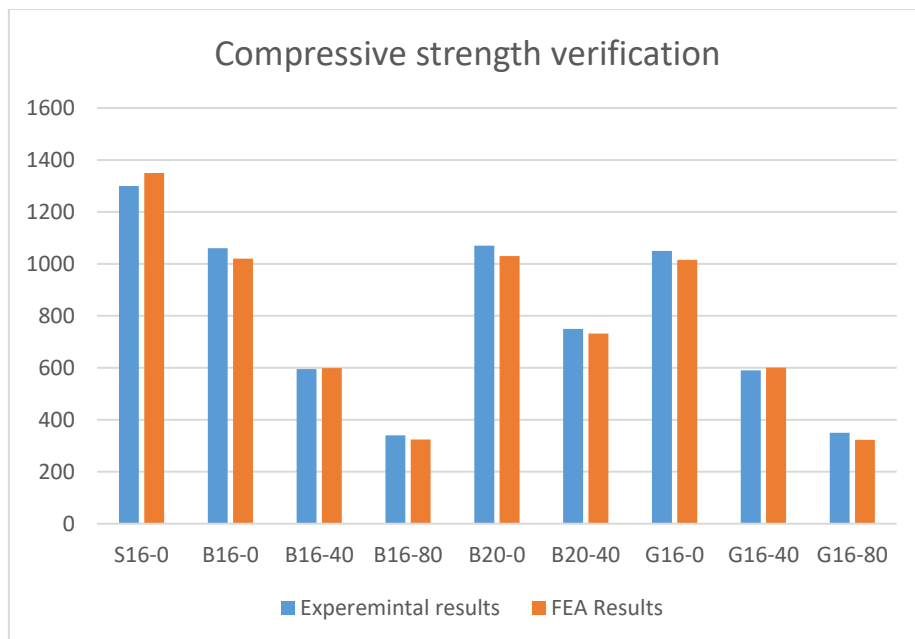


Figure 4.6: Comparison between experimental and FEA results

Figure 4.7 shows the force-displacement diagram for the experimental work and the FE modeling.

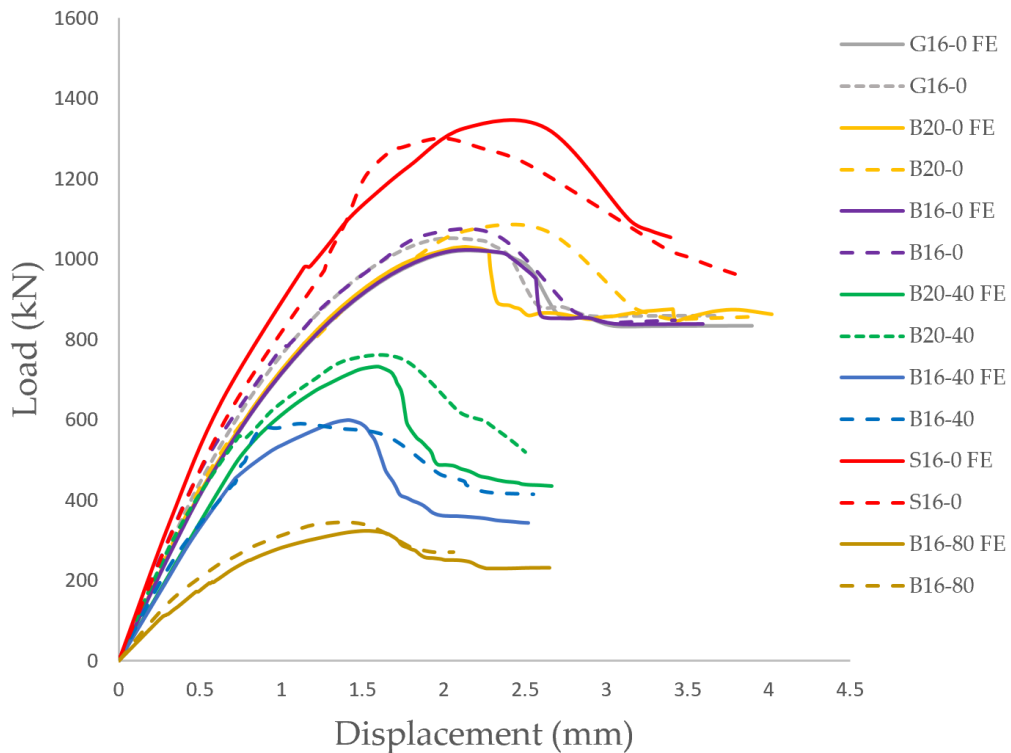


Figure 4.7: Load vs displacement comparison between experimental work and FE modelling

4.1.4 Parametric analysis: Performance of GFRP- and BFRP-RC columns.

A parametric study was conducted to further investigate the response of the GFRP and BFRP bars in RC columns by considering different reinforcement ratios, shapes and dimensions, concrete compressive strengths, and stirrups types. The outcome of changing these parameters on the overall behavior of the RC columns is also presented and discussed. Two different column geometries with rectangular and circular cross-sections were investigated, as shown in Figure 4.8 and Figure 4.9, respectively.

Figure 4.8 represents the column detail for rectangular cross sections. For all the rectangular sections, 4 bars were used, and the reinforcement ratio was increased by increasing the bar diameter to reach the required reinforcement ratio. It should be noted that bar diameters were selected based on the availability of actual cross bar diameters available in the market.

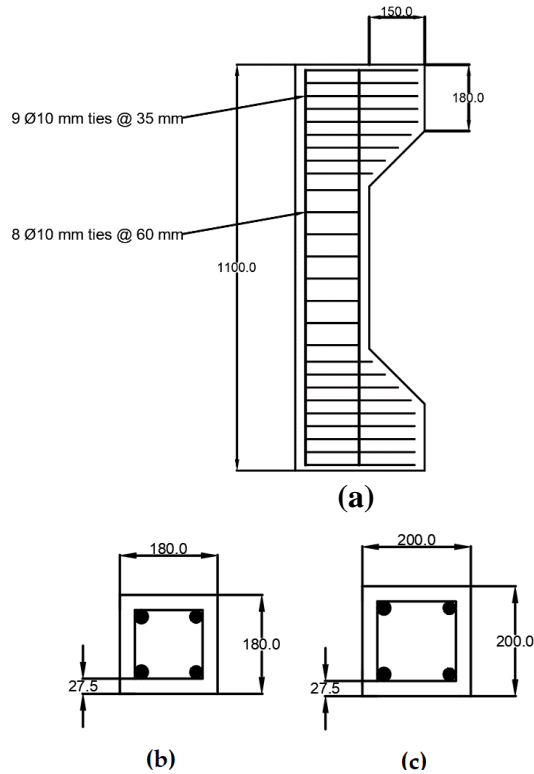


Figure 4.8: Rectangular FRP-RC column details: (a) column dimensions (b) cross section of 180 mm x 180 mm column (c) cross section of 200 mm x 200 mm column

Figure 4.9 represents the column detail for circular cross sections. For all the circular sections, 6 bars were used, and the reinforcement ratio was increased by increasing the bar diameter to reach the required reinforcement ratio. A cover of 27.5 mm was used for all columns, the spacing of the shear stirrups is shown in Figure 4.9, and the total length of columns modelled was 1100mm.

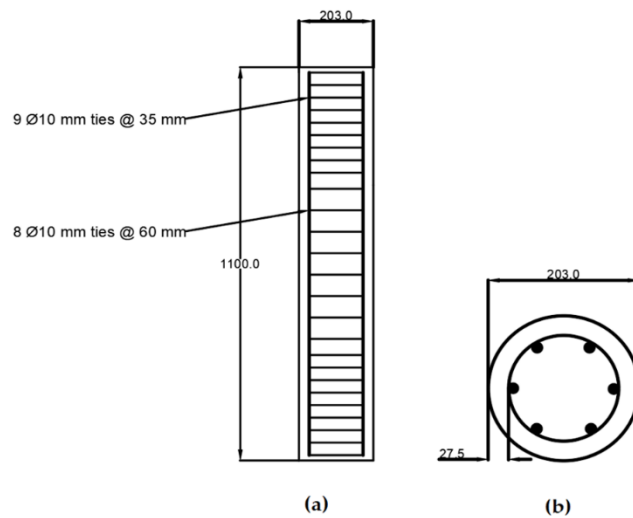


Figure 4.9: Circular FRP-RC column detail of 203 mm diameter (a) column dimension (b) cross section

A number of FE models were developed for several reinforcement ratios and varying eccentricities to develop interaction diagrams. In the first step in producing interaction diagrams of the same reinforcement ratio, columns were modelled under various eccentricities, starting from the maximum eccentricity up to pure concentric loading. Another parameter in this study is the concrete strength, which was varied to study its effect on the columns' behavior.

The columns in the FEA parametric study were divided into ten groups. Each group includes a total of forty-five (45) short RC columns of 1%, 2%, 4%, 6% and 8% reinforcement ratio. Group 1 columns have square cross-sections, GFRP as a main reinforcement with 180 mm width, steel ties, and an ultimate concrete strength of 40 MPa; Group 2 columns have square cross-sections, GFRP as a main reinforcement with 180 mm width, GFRP ties, and an ultimate concrete strength of 40 MPa; Group 3 columns have square cross-sections, GFRP as a main reinforcement with 200 mm width, steel ties, and an ultimate concrete strength of 40 MPa; Group 4 columns have square cross-sections, BFRP as a main reinforcement with 180 mm width, steel ties, and an ultimate concrete strength of 40 MPa; Group 5 columns have square cross-sections, BFRP as a main reinforcement with 180 mm width, BFRP ties, and an ultimate concrete strength of 40 MPa; Group 6 columns have square cross-sections, BFRP as a main reinforcement with 200 mm width, steel ties, and an ultimate concrete strength of 40 MPa; Group 7 columns have circular cross-sections, BFRP as a main reinforcement with 200 mm diameter, steel stirrups, and an ultimate concrete strength of 40 MPa; Group 8 columns have square cross-sections, GFRP as a main reinforcement with 180 mm width GFRP ties, and an ultimate concrete strength of 30 MPa; Group 9 columns have circular cross-sections, BFRP as a main reinforcement with 200 mm diameter, GFRP stirrups and an ultimate concrete strength of 40 MPa, and finally Group 10 columns have circular cross-sections, GFRP as a main reinforcement with 200 mm diameter, steel stirrups, and an ultimate concrete strength of 30 MPa.

All parametric analysis results were extracted from ABAQUS FE modelling. For the same reinforcement ratio, nine (9) FEA models were analyzed, including one with pure concentric loading and one with pure moment, and then an interaction diagram was drawn to measure the change in combined axial and flexural capacity when the eccentricity is changed. Several FEA models were studied using ABAQUS,

and the column dimension, column reinforcement ratio, column cross-sectional shape, and material used for ties was varied. Table 4.2 explains the parametric study groups. A total number of 450 reinforced columns were modeled to study their compressive behavior. Within the group, each column has a unique ID.

The columns in the FE parametric study were divided into ten groups. Each group consisted of a total of 45 short RC columns, including a total of nine load eccentricities with five reinforcement ratios of 1%, 2%, 4%, 6%, and 8% for each load eccentricity, as listed in Table 4.2.

Table 4.2: Parametric study groups table

Group	Column ID	Cross-Sectional Shape	Main Reinforcement Material	Dimensions (B or D) (mm)	Ties Material	fc' (MPa)	Eccentricity
Group-1	S-G180-S**-40	Square	GFRP	180	Steel	40	
Group-2	S-G180-G**-40	Square	GFRP	180	GFRP	40	
Group-3	S-G200-S**-40	Square	GFRP	200	Steel	40	
Group-4	S-B180-S**-40	Square	BFRP	180	Steel	40	0,10,20,30,40,60,80,100 and Pure Moment
Group-5	S-B200-S**-40	Square	BFRP	200	Steel	40	
Group-6	S-B200-B**-40	Square	BFRP	200	BFRP	40	
Group-7	S-G180-S**-30	Square	GFRP	180	GFRP	30	
Group-8	C-B200-S**-40	Circular	BFRP	203	Steel	40	
Group-9	C-B200-G**-40	Circular	BFRP	203	GFRP	40	
Group-10	C-B200-S**-30	Circular	BFRP	203	Steel	30	

Note: ** denotes 00, 10, 20, 30, 40, 60, 80, 100, and Pure Moment, which corresponds to the eccentricity

Each column was labeled with a unique ID in each group. The first letter indicates the column cross-section type (S for square cross-section, and C for circular cross-section); the second letter refers to the type of reinforcement (G for GFRP, B for

BFRP); the number after the second letter provides information about the width/diameter of the cross sectional area; the following letter denotes the tie material (S for steel, G for GFRP, and B for BFRP), followed by the eccentricity in mm; and, finally, the last number provides information about the concrete compressive strength used. As an example, S-G180-S80-40 indicates a square column of 180 mm width, reinforced with GFRP bars and steel ties, has a concrete compressive strength of 40 MPa, and loaded at 80 mm eccentricity.

The main objective of considering the 10 groups listed in Table 4.2 was to investigate the effect of the different parameters on the overall responses of the FRP-RC columns and their interaction diagrams. For example, the difference between Group 1 and Group 2 is only the type of ties material (steel vs. GFRP) and the difference between Group 1 and Group 3 was the dimension of the square cross-section (180 mm vs. 200 mm). Furthermore, the concrete compressive strength considered for Group 10 was 30 MPa while the concrete compressive strength for the other nine groups was 40 MPa. The 450 columns were numerically analyzed, and the results were reported and discussed.

Figure 4.10 presents a sample of the load vs. displacement curves for columns of the 1% reinforcement ratio in Group 1, predicted using the FE models.

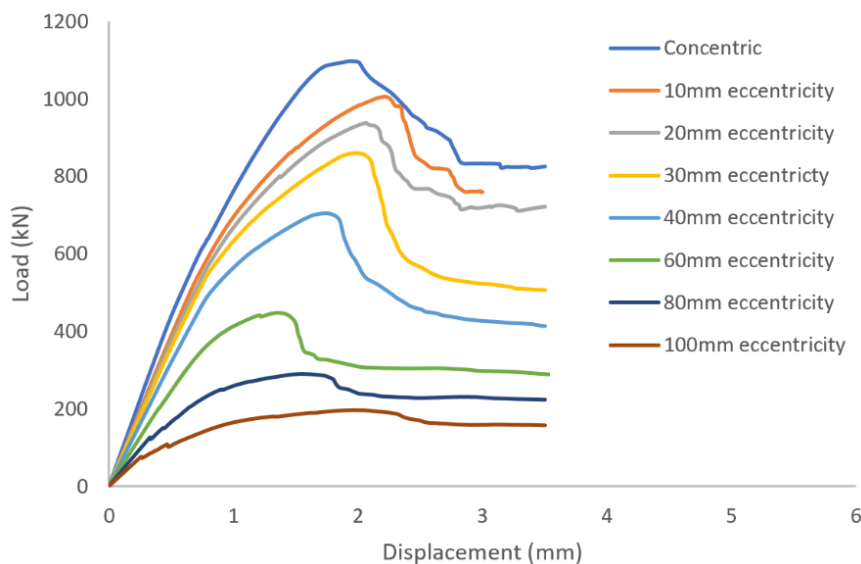


Figure 4.10: Load vs. displacement results for columns in Group 1, at the 1% reinforcement ratio.

The results clearly illustrate the transition in the stiffness of the columns as well as ultimate compressive loads over the different eccentricities considered. After obtaining the load vs. displacement results for all groups, interaction diagrams were developed for the five different reinforcement ratios, as shown in Figure 4.11, Figure 4.12, Figure 4.13, Figure 4.14, Figure 4.15, Figure 4.16, Figure 4.17, Figure 4.18, Figure 4.19 and Figure 4.20, which correspond to the columns in Groups 1–10, respectively.

An interaction diagram can be defined as a curve that shows the interaction between axial force and bending moment in which an acceptable capacity of a column with similar properties can be classified as safe for carrying that set of loads combination. Pure axial compressive load is the point at which the R_n value is equal to zero at zero eccentricity, while pure flexure is the point at which the K_n value is equal to zero.

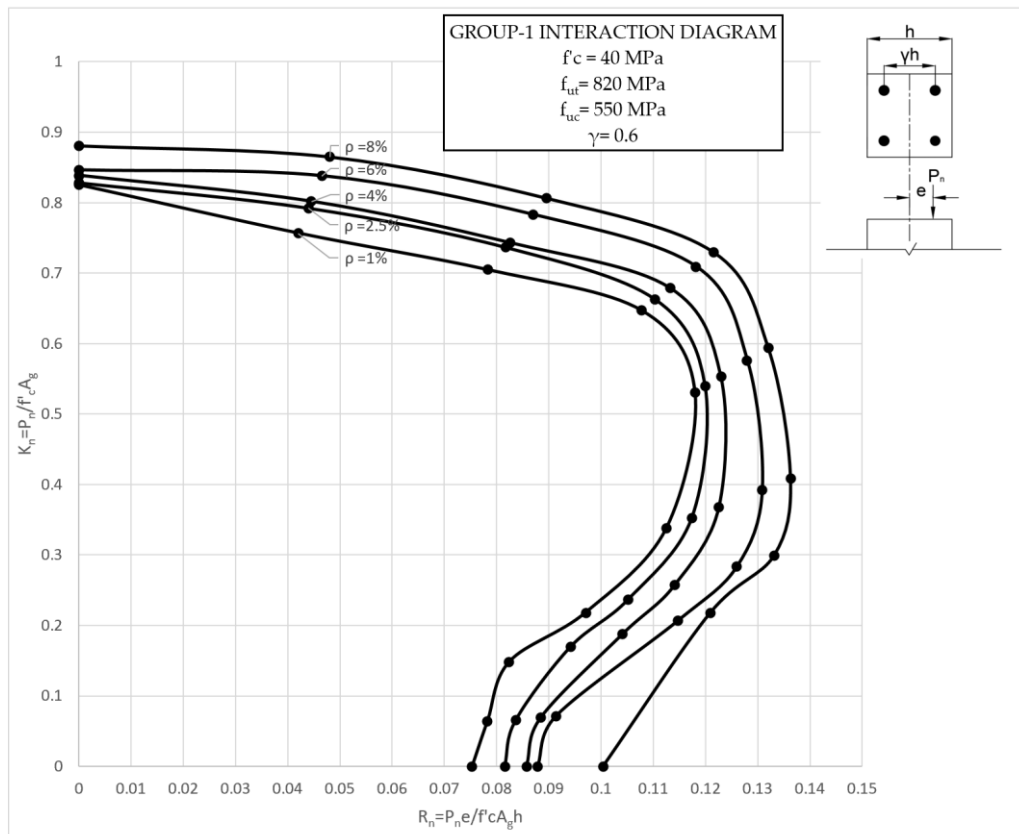


Figure 4.11: Group-1 interaction diagram

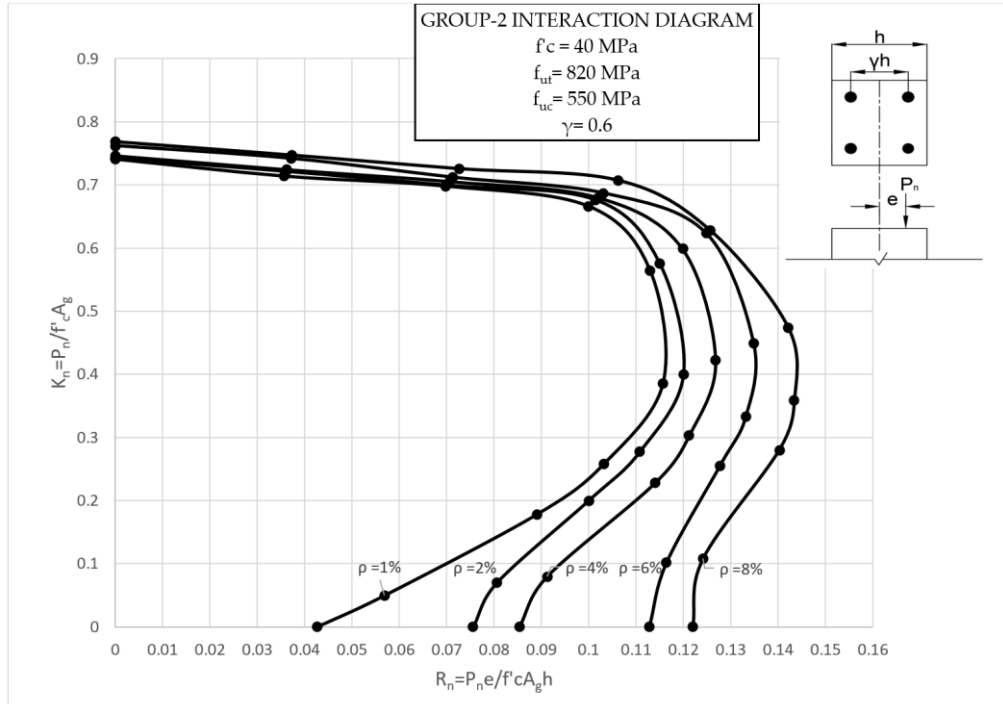


Figure 4.12: Group-2 interaction diagram

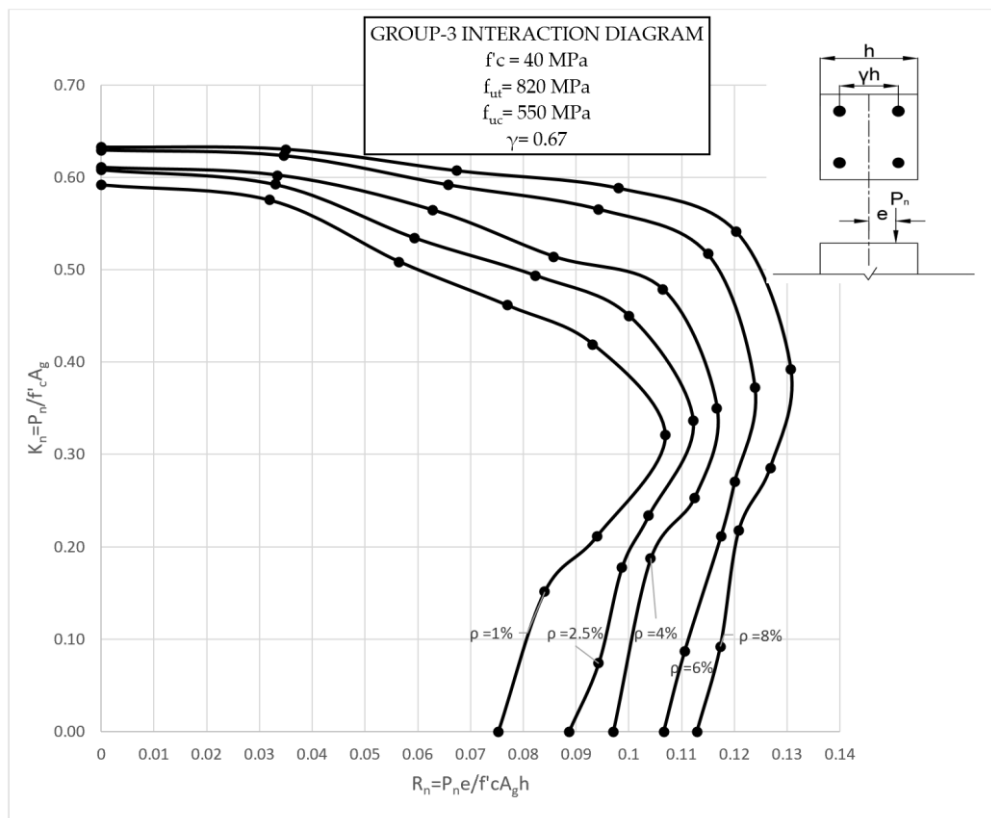


Figure 4.13: Group-3 interaction diagram

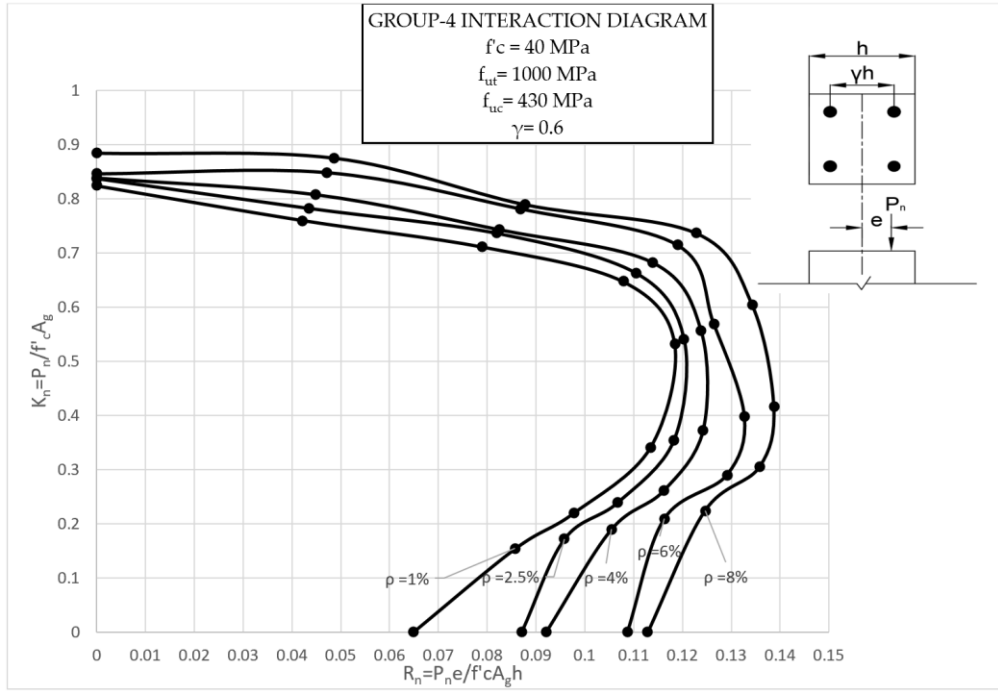


Figure 4.14: Group-4 interaction diagram

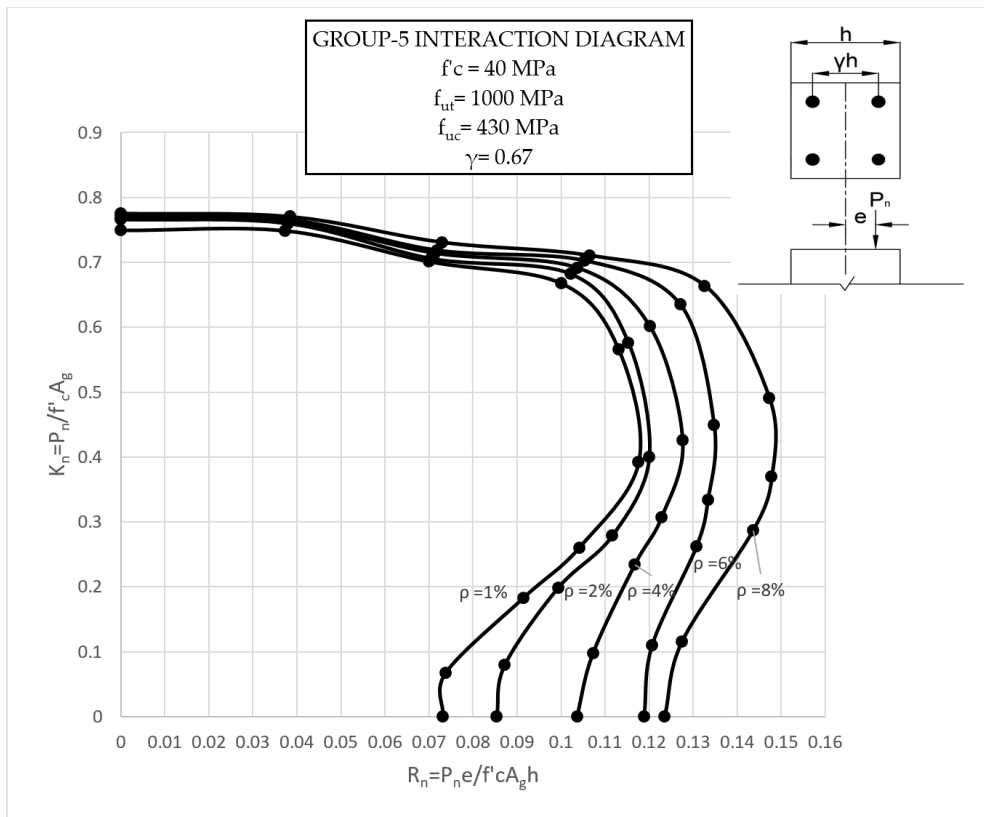


Figure 4.15: Group-5 interaction diagram

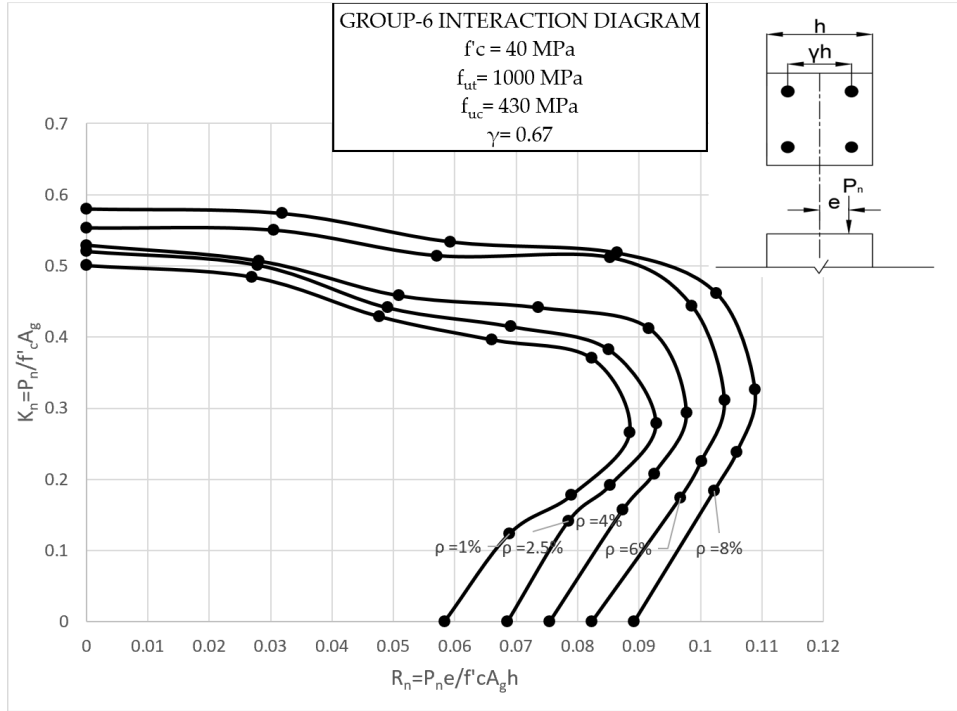


Figure 4.16: Group-6 interaction diagram

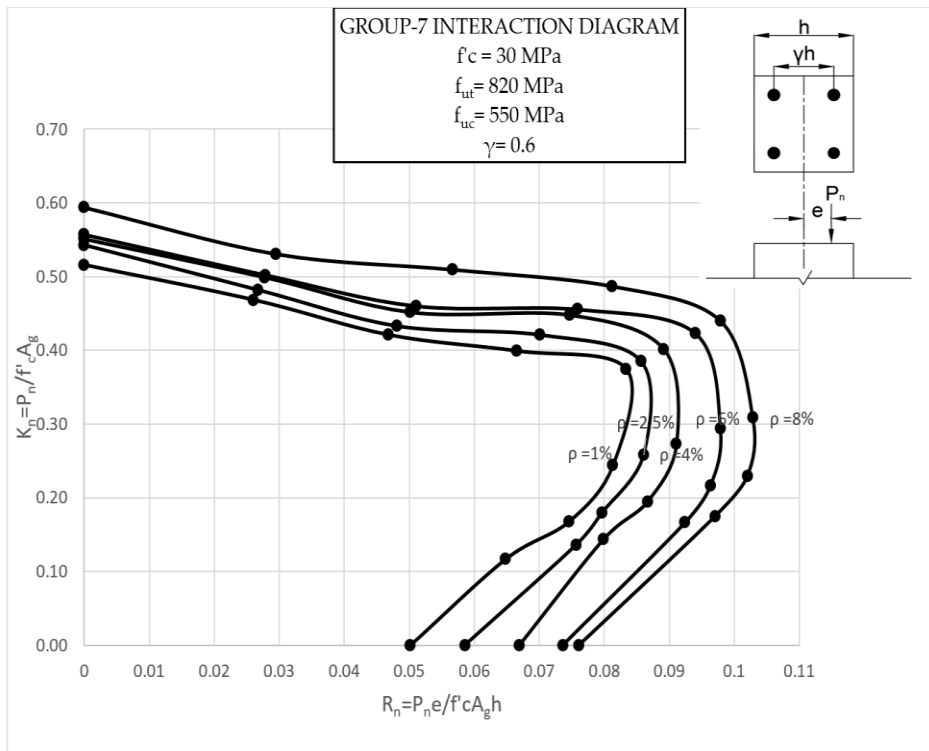


Figure 4.17: Group-7 interaction diagram

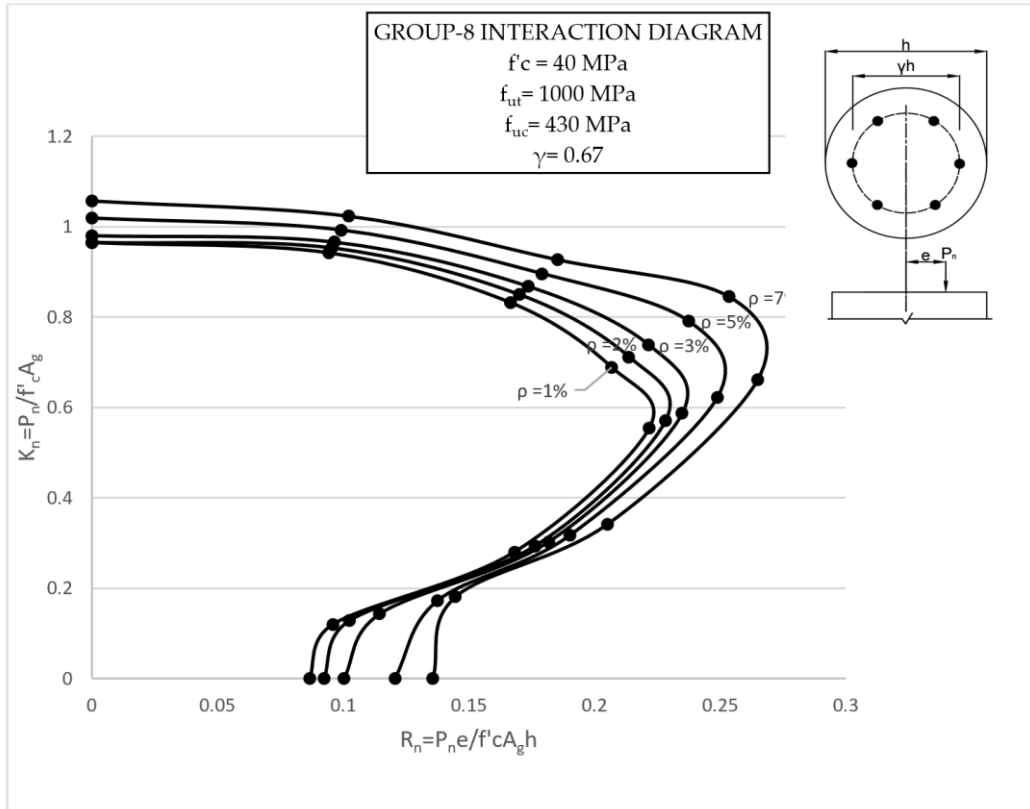


Figure 4.18: Group-8 interaction diagram

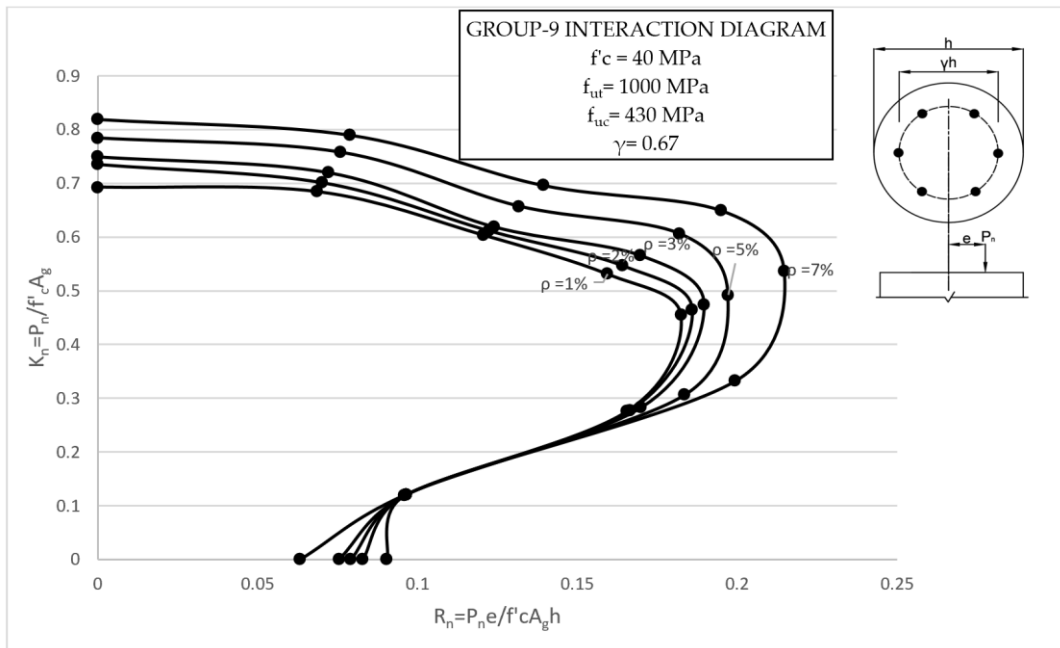


Figure 4.19: Group-9 interaction diagram

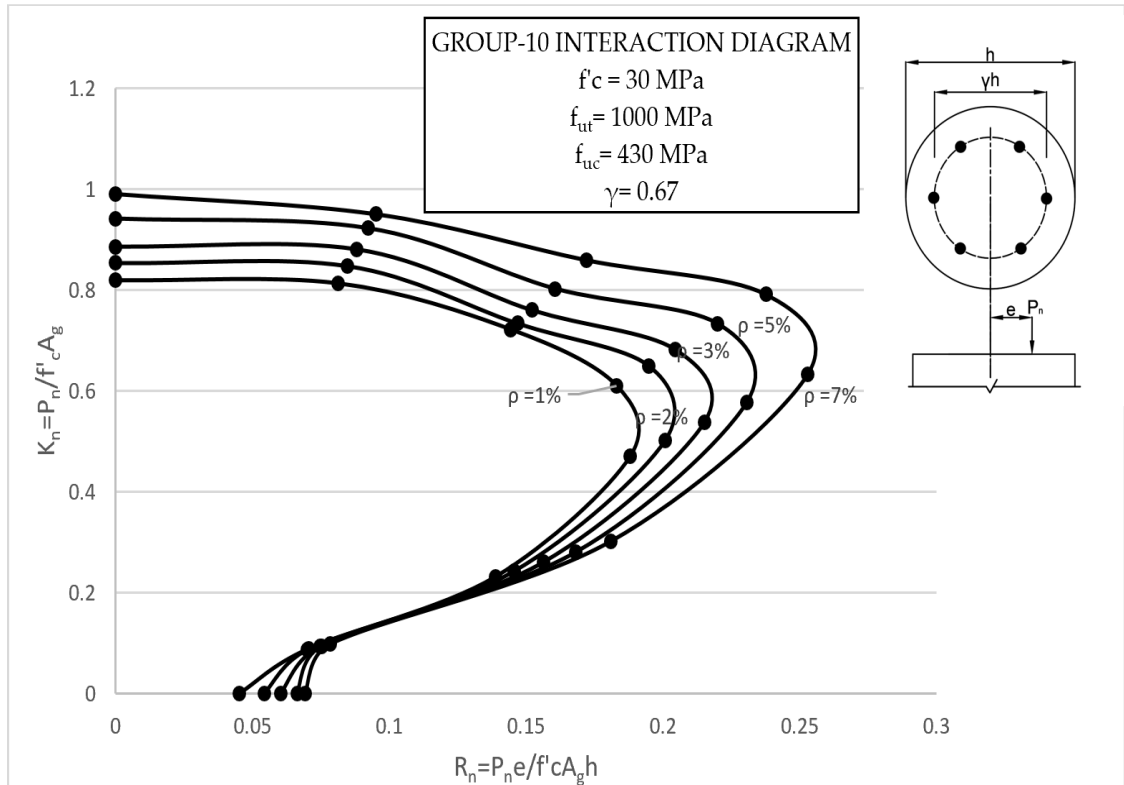


Figure 4.20: Group-10 interaction diagram

The overall response and shape of these interaction diagrams were similar to the graphs presented in the ACI 318 [58] for steel-reinforced RC columns. In Figure 4.11, Figure 4.12, Figure 4.13, Figure 4.14, Figure 4.15, Figure 4.16, Figure 4.17, Figure 4.18, Figure 4.19 and Figure 4.20 provide valuable information for the design of GFRP- and BFRP-RC columns.

The axial load vs. displacement results were also utilized to study the contribution of the GFRP and BFRP bars to the total compressive strength of the concentric FRP-RC columns in all groups. The confined concrete strength factor and ductility indices for the concentric FRP-RC columns were also calculated and compared. The confined concrete strength factor (f'_{cc}) was calculated for each column as the difference between the peak load and force carried by the bars, divided by the confined concrete area (A_c) delineated by the centerline of the ties ($(P_{max} - P_{bar}) / A_c$). Values of the confined concrete strength factor (f'_{cc}) for concentrically loaded columns are shown in Table 4.3.

Table 4.3: Confined concrete strength factors and ductility indices of all concentric columns

Column ID	Reinforcement Ratio	P_{max}	f'_{cc}	DI	$P_{concrete}$	$P_{concrete}/P_{max}$	P_{bar}/P_{max}
S-G180-S00-40	1%	1096	52.5	1.86	1042	0.95	0.05
	2%	1100	51.5	1.66	1004	0.91	0.09
	4%	1114	50.7	1.41	965	0.87	0.13
	6%	1126	52.5	1.43	963	0.85	0.15
	8%	1170	54	1.56	964	0.82	0.18
S-G180-G00-40	1%	841	40.8	1.32	810	0.96	0.04
	2%	865	41.8	1.5	816	0.94	0.06
	4%	868	41.4	1.33	789	0.91	0.09
	6%	895	42.1	1.35	772	0.86	0.14
S-G200-S00-40	8%	899	42.2	1.41	754	0.84	0.16
	1%	1114	41.6	2.02	1080	0.97	0.03
	2%	1218	46	1.55	1157	0.95	0.05
	4%	1224	44.6	1.96	1109	0.91	0.09
	6%	1250	44.4	2.01	1064	0.85	0.15
S-B180-S00-40	8%	1260	43.9	2.2	1018	0.81	0.19
	1%	1095	53.2	1.56	1056	0.96	0.04
	2%	1113	53.5	1.43	1044	0.94	0.06
	4%	1114	50.7	1.63	965	0.87	0.13
	6%	1124	52.2	1.58	957	0.85	0.15
S-B200-S00-40	8%	1175	54.1	1.68	966	0.82	0.18
	1%	1228	45.3	1.33	1177	0.96	0.04
	2%	1256	47.5	1.34	1196	0.95	0.05
	4%	1258	46.3	1.3	1152	0.92	0.08
S-B200-B00-40	6%	1265	45.1	1.39	1080	0.85	0.15
	8%	1271	44.4	1.43	1030	0.81	0.19
	1%	811	40.2	2.13	785	0.97	0.03
	2%	843	41.7	1.46	812	0.96	0.04
S-G180-S00-30	4%	857	42.2	1.93	803	0.94	0.06
	6%	896	43.6	2.02	800	0.89	0.11
	8%	940	44	2.13	786	0.84	0.16
	1%	685.8	32.8	2.08	652	0.95	0.05
	2%	721	33.8	2.02	660	0.92	0.08
C-B200-S00-40	4%	732	34.1	1.96	650	0.89	0.11
	6%	740	34.7	2.12	636	0.86	0.14
	8%	789	34.1	2.27	609	0.77	0.23
	1%	1281	102.2	2.07	1267	0.99	0.01
C-B200-S00-40	2%	1285	90.9	2.01	1109	0.86	0.14
	3%	1301	89	1.84	1063	0.82	0.18
	5%	1352	91.8	2.24	1041	0.77	0.23
	7%	1403	93.9	2.47	994	0.79	0.21
	1%	920	64.4	2.1	799	0.87	0.13

C- B200- G00-40	2%	976	65.8	2.2	802	0.82	0.18
	3%	995	66.4	2.24	794	0.8	0.20
	5%	1041	66.8	2.38	758	0.73	0.27
	7%	1087	71.5	2.45	756	0.7	0.3
	1%	1087	81	2.17	1005	0.92	0.08
C- B200- S00-30	2%	1133	81.9	2.25	999	0.88	0.12
	3%	1176	85.8	2.51	1025	0.87	0.13
	5%	1249	89.5	2.45	1015	0.81	0.19
	7%	1315	94.3	2.67	998	0.76	0.24

Ductility is a desired property in structural design as it protects structures against unpredicted overloading and/or load reversals. It is therefore essential that RC columns possess adequate ductility. Ductility can be achieved if a sufficient amount of later reinforcement is used in reinforcing RC columns, afterwards. A method was developed by Pessiki and Peironi [63] in which the column ductility is calculated as the ratio of the ultimate axial displacement (δ_u) to the yield axial displacement (δ_y), given by $DI = \delta_u/\delta_y$. In this method, the yield displacement is estimated to be the axial displacement corresponding to the yield load or to the limit of the linear behavior. The ultimate displacement is assumed to be the axial displacement at 85% of the peak load in the post-peak descending portion of the load vs. displacement curve. The ductility index (DI) for the column is then calculated as the ratio of the displacements obtained for all columns, as shown in Table 4.3.

Additionally, values of the force carried by the concrete ($P_{concrete}$), calculated as the difference between the ultimate load (P_{max}) and the load carried by the bars (P_{bar}), are shown in Table 4.3 for all the concentric columns.

A comparison is also conducted between the Analytical method using the design equations of the ACI 318 [58] and the FE modelling for the 1% reinforcement ratio of group 1, as shown in Figure 4.21.

It shall be noted that the ACI 318 [58] equations was used without applying the load reduction factors, since these factors are introduced for safety purposes to account for long term durability of the concrete structures and also to account for manufacturing or production variety in both concrete material and steel material, since there is no perfect production for material.

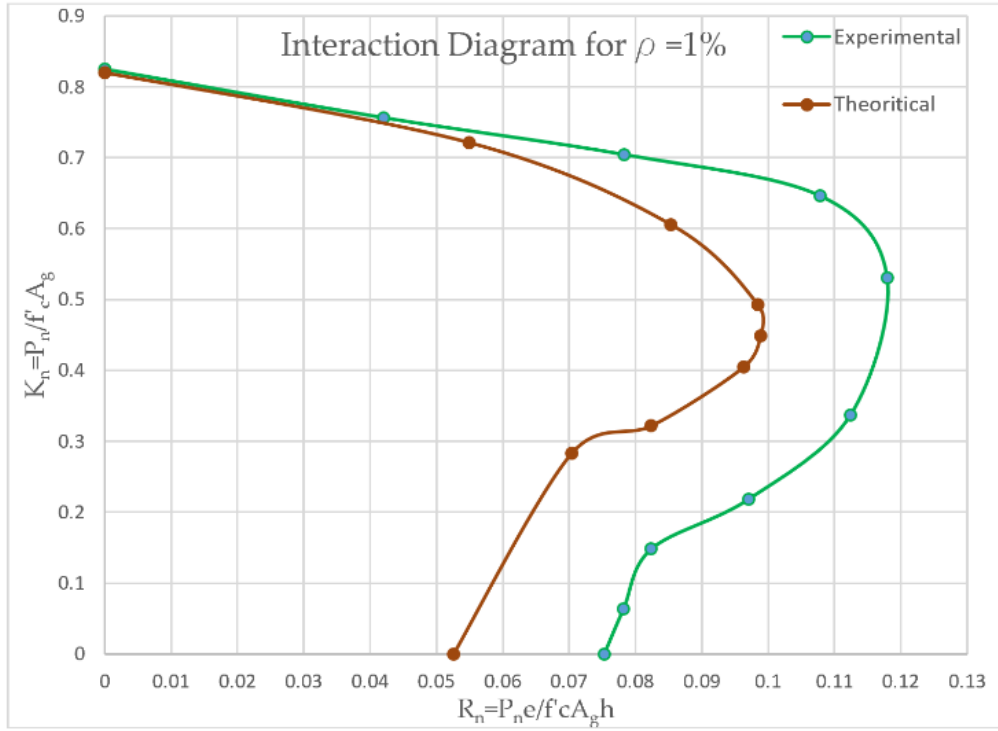


Figure 4.21: Theoretical as per ACI318 [58] vs experimental interaction diagram for group-1 (1%).

Chapter 5. Discussion of Results

In this chapter, a detailed discussion and analysis of the results presented in the previous chapters is provided. The effects of each of the finite element parameters on the overall behavior of the columns are discussed. This is followed by explanations of the finite element axial load-bending moment interaction diagrams and parametric study discussion. Finally, the design equations currently proposed by FRP RC design codes and by other studies from the literature review are evaluated in light of the results obtained from this study.

Group 1 columns were modelled to study the effects of the longitudinal reinforcement ratio and eccentricity on the overall behavior of the columns. The maximum axial loads were sustained by specimens of the highest reinforcement ratio and zero eccentricity, but also increasing the GFRP longitudinal reinforcement ratio has insignificant effect on strength. The contributions of the bars to the ultimate columns capacities, reported as $P_{\text{bar}}/P_{\text{max}}$ in Table 4.3, were calculated by multiplying the measured average axial stress in the longitudinal bars with the total cross-sectional area of the bars. Using those measured stress values, the average contribution to the ultimate column capacity of the 12 mm GFRP bars was calculated as 4.9% and 8.7% for the 16 mm diameter GFRP bars, 13.4% for the 20 mm diameter GFRP bars, 14.5% for the 25 mm diameter GFRP bars and 17.6% for the 28 mm diameter GFRP bars. The maximum axial load sustained by the column longitudinally reinforced with GFRP bars was 1170 kN, which is only 3% lower than its counterpart column longitudinally reinforced with BFRP bars. The average bars contribution to the ultimate column's capacity was calculated as 12.6%.

5.1. Effects of Parameters on the Overall Behavior of FRP RC Columns

The parameters investigated in this study include the longitudinal reinforcement type (steel, BFRP and GFRP bars), cross sectional shape (square, round), cross sectional area, ties reinforcement material and concrete strength. To investigate the effects of changing each of these parameters on the overall behavior of RC columns, graphs of axial load versus axial displacements are compared for all columns. Also, the confined concrete strength factor and ductility indices for the concentric columns were calculated and compared. The confined concrete strength factor (f'_{cc}) was calculated for each column as the difference between peak load and force carried by bars, divided

by the confined concrete area (A_c) delineated by the centerline of the ties ($(P_{max} - P_{bar})/A_c$). Values of the confined concrete strength factor (f'_{cc}) for concentrically loaded columns are shown in Table 4.2.

Ductility is defined as the ability of a material to undergo inelastic deformations with acceptable stiffness and strength reduction [64]. Ductility is a desired property in structural design as it protects structures against unpredicted overloading and/or load reversals. It is therefore essential that RC columns possess adequate ductility. A method was developed by Pessiki and Peironi [63] in which the column ductility is calculated as the ratio of the ultimate axial displacement (δ_u) to the yield axial displacement (δ_y), given by:

$$DI = \delta_u / \delta_y$$

This method was adopted in this study. In this method, the yield displacement is estimated to be the axial displacement corresponding to the yield load or to the limit of the linear behavior. The ultimate displacement is assumed to be the axial displacement at an axial load level of 85% of the peak load in the post-peak descending portion of the axial load-axial displacement curve. The 85% peak load, which was used for comparison purposes, is a reasonable limit at which it can be considered that a column has maintained its ultimate resistance, as explained in Pessiki and Peironi [22]. For each concentric column specimen, a horizontal line to the peak load of the column is plotted, in addition to plotting a best-fit line to the initial linear portion of the load-displacement curve. The displacement of the intersection of these two lines is labelled as displacement corresponding to the limit of elastic behavior (δ_y).

While the ultimate axial displacement (δ_u) can be obtained by plotting a horizontal line at 85% of peak load, the displacement corresponding to the intersection of the descending portion of the load-displacement curve with this line is labelled as (δ_u). After that, the ductility index for the column was calculated as the ratio of the displacements obtained. Values of the ductility indices (DI) for all columns are shown in Table 4.3.

An illustration of the calculation is shown in Figure 5.1.

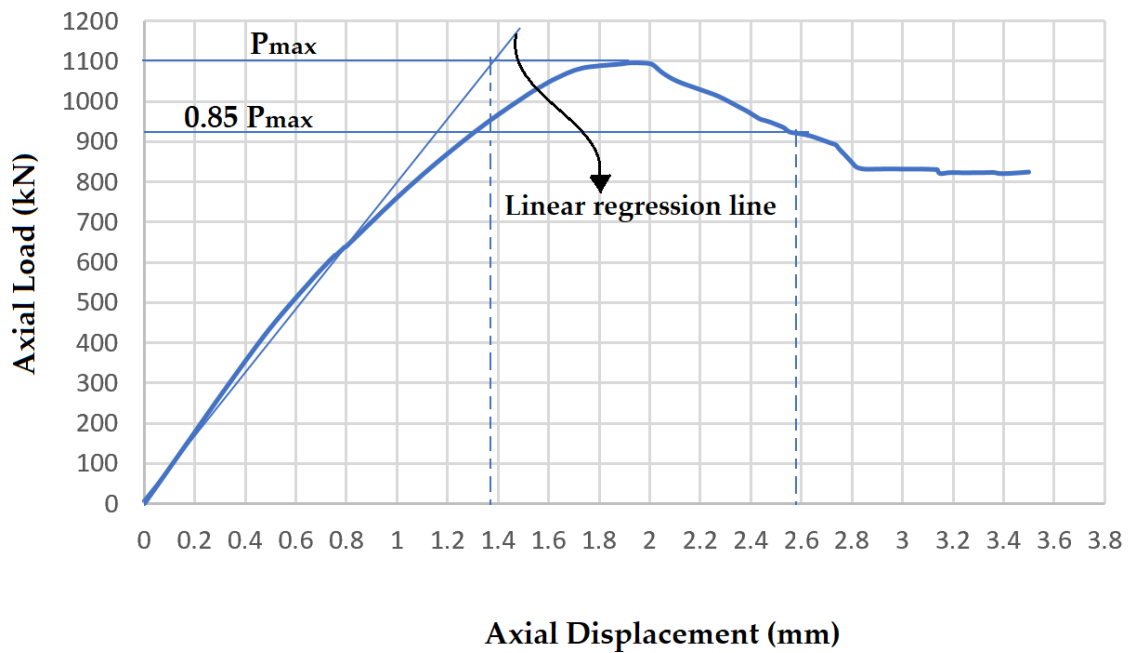


Figure 5.1: Determination of displacements for calculating columns ductility index (graph of column ID S-G180-S00-40 1%)

Also, values of the force carried by the concrete ($P_{concrete}$), calculated as the difference between the ultimate load (P_{max}) and the load carried by the bars (P_{bar}), are shown in Table 4.3 for all concentric columns.

5.2. Effect of Longitudinal Reinforcement Type and Ratio

Column specimens in groups 1 to 10, were designed to study the effect of different GFRP and BFRP longitudinal reinforcement ratios of 1% to 8%. The results show that the columns with a larger longitudinal reinforcement ratio attain higher ultimate capacities than their counterparts with lower reinforcement ratio, at all eccentricity values. For all groups, the differences in the ultimate capacities between the columns generally increase as the load eccentricity increases such that specimens in group 4 having reinforcement ratios of 8% show axial capacities higher than those with reinforcement ratios of 1%, as shown in Figure 5.2.

Additionally, the strength contribution of main bars to the ultimate column capacity was found to be higher for columns with a higher reinforcement ratio when compared to the lower reinforcement ratio, as shown in Table 4.3.

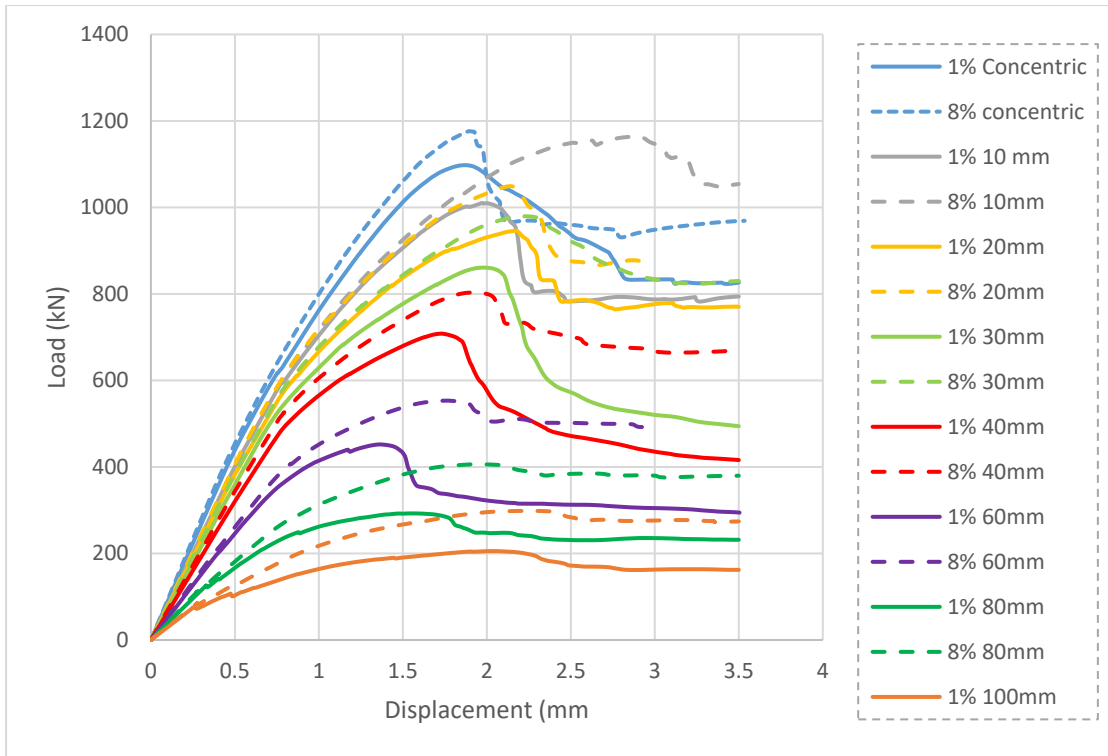


Figure 5.2: Group-4 force vs displacement For 1% and 8% reinforcement ratio

This is a result of the higher ultimate stresses reached in the higher diameters of main reinforcement and their larger cross-sectional area, as compared to the lower diameter bars. Moreover, specimens with larger reinforcement ratios showed larger axial displacements at peak loads than those with smaller reinforcement ratios. An example of this is illustrated in Figure 5.2.

Also, column ductility was higher for lower reinforcement ratios than for higher ones, as shown in Table 4.3.

5.3. Effect of Cross-Sectional Shape and Dimension

The results show that the columns with a larger cross section attain higher ultimate capacities than their counterparts with a smaller cross section at all eccentricity values. The ductility was almost similar for the larger and smaller cross sections.

Additionally, the results show that circular cross sections attain significantly higher ultimate capacities than square cross sections for the same cross sectional area. Circular cross sections also have higher ductility than the square cross sections. For example, when comparing group 1 and group 8, all concentric group 8 (circular

columns) had a higher ductility, while the ultimate capacity of group 8 was higher than group 1 by the range of 16 to 20%.

5.4. Effect of Transverse Reinforcement Type

Column specimens of groups 2, 7 and 9 were developed to study the effects of using GFRP ties as compared to steel ties on the overall behavior of the columns, while group 6 was developed to study the effects of using BFRP ties on the overall behavior of the columns. Lateral reinforcement improves the strength and ductility of confined concrete, as concrete can be improved to a large extent through the use of lateral reinforcement [65]. In this study, all groups are transversely reinforced with ties at 60 mm spacing. The columns that are confined with steel ties showed higher axial capacities than the ones confined with GFRP or BFRP ties. In addition, concentric columns reinforced with steel ties had higher confined concrete strength than the ones confined with GFRP or BFRP ties, as shown in Table 4.3.

Additionally, the results show that columns confined with steel ties achieved higher ductility than those confined with BFRP ties at concentric loads.

For example, comparing columns in groups 1 and 2 at 1% reinforcement ratio, where all the variables/parameters except the lateral reinforcement are similar, the maximum axial capacities were 1096 kN and 841 kN for columns in group 1 and group 2, respectively, while the ductility indices for the same reinforcement ratio were 1.96 and 1.32 for columns in group 1 and group 2, respectively.

Furthermore, the confined concrete strength factor (f'_{cc}) was significantly higher for columns with steel lateral reinforcement. For example, the confined concrete strength factor for columns in group 1 was, on average, 25% higher (f'_{cc}) than the ones in group 2.

5.5. Interaction Diagrams

After verifying the FE models, the interaction diagram can be produced by setting several important points. The succession of points is based on the value of maximum compressive load. Eight loading conditions were considered, concentric loading, loading under 10, 20, 30, 40, 60, 80 and 100 mm eccentricities, and a pure-moment case. Failure is either initiated by the rupture of FRP bars in tension (ϵ_f) or by concrete crushing (ϵ_c) which are referred to, respectively, as tension-controlled and

compression-controlled failure modes. Figure 5.3 represents the rectangular column cross sectional strain diagram.

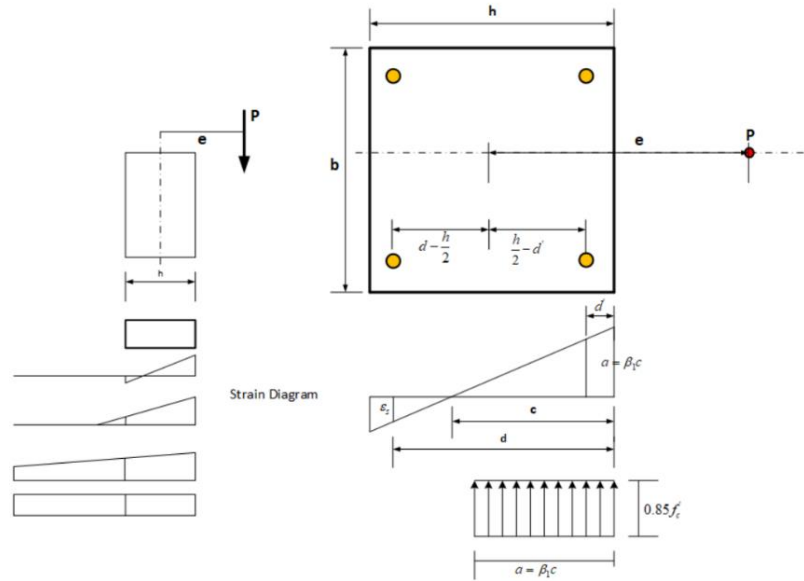


Figure 5.3: Rectangular column cross sectional strain diagram

The analytical results of the study were utilized to plot normalized axial load-bending moment (P-M) interaction diagrams for all groups in terms of normalized axial force (K_n) and normalized bending moment (R_n). The K_n and R_n values are calculated as:

$$K_n = P_n f'_c A_g \quad (5.1)$$

$$R_n = P_n e f'_c A_g h \quad (5.2)$$

where, P_n = ultimate axial load carried by column,

f'_c = concrete compressive strength,

A_g = column's gross sectional area,

h = column dimension, and

e = initial applied eccentricity value

The normalized axial load-bending moment interaction diagrams are shown in Figure 4.11 to Figure 4.20 for columns of groups 1 to 10. Nine points were used to develop the P-M curves for each set of columns. The first point represents the column

tested under concentric loads, and then the successive 7 points represent the column specimens tested under 10, 20, 30, 40, 60, 80 and 100 mm eccentricities, respectively. The last point represents pure moment.

Predominantly, columns in all groups were controlled by concrete crushing (compression controlled) since concrete is controlling the behavior. At failure, the concrete exhibited high plastic strain values, beyond 0.003, while, the main reinforcement did not develop any plastic strain, which indicates that the GFRP and BFRP bars, unlike steel, did not yield.

5.6. Evaluation of Proposed Design Equations for FRP RC Columns

Several design equations have been proposed in the literature to determine the ultimate axial capacities of concentric reinforced short RC columns with FRP, as shown in Table 2.3. The results of the predicted axial capacities of the columns tested in this study, as calculated by each of the proposed equations, in comparison with the experimental axial capacities, are illustrated by the bar charts shown in Figure 5.4, Figure 5.5, Figure 5.6, Figure 5.7, Figure 5.8, Figure 5.10 and Figure 5.10.

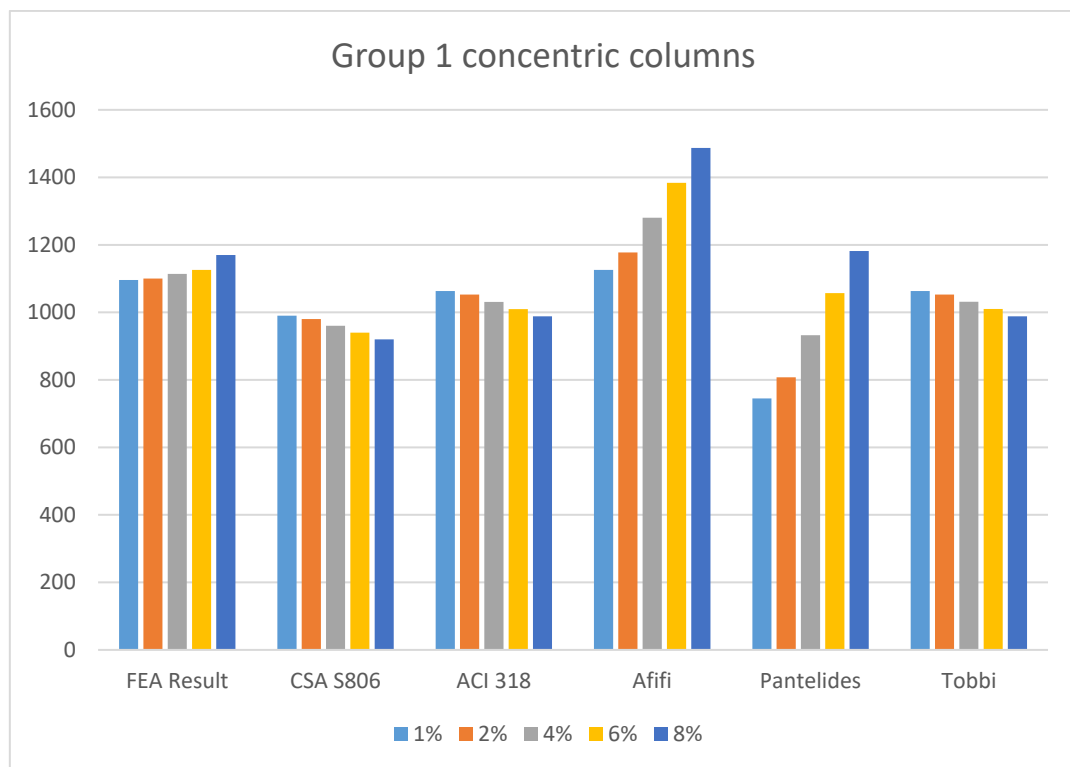


Figure 5.4: Group 1 FEA results comparison with proposed short columns equations

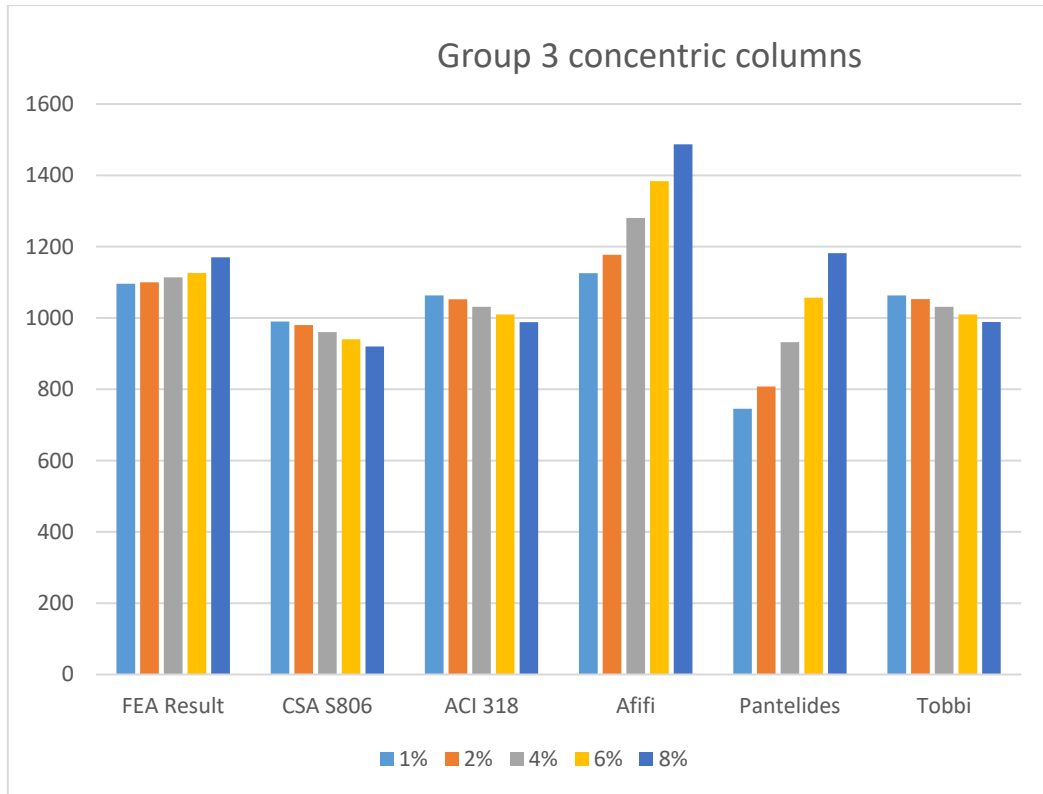


Figure 5.5: Group 3 FEA results comparison with proposed short columns equations

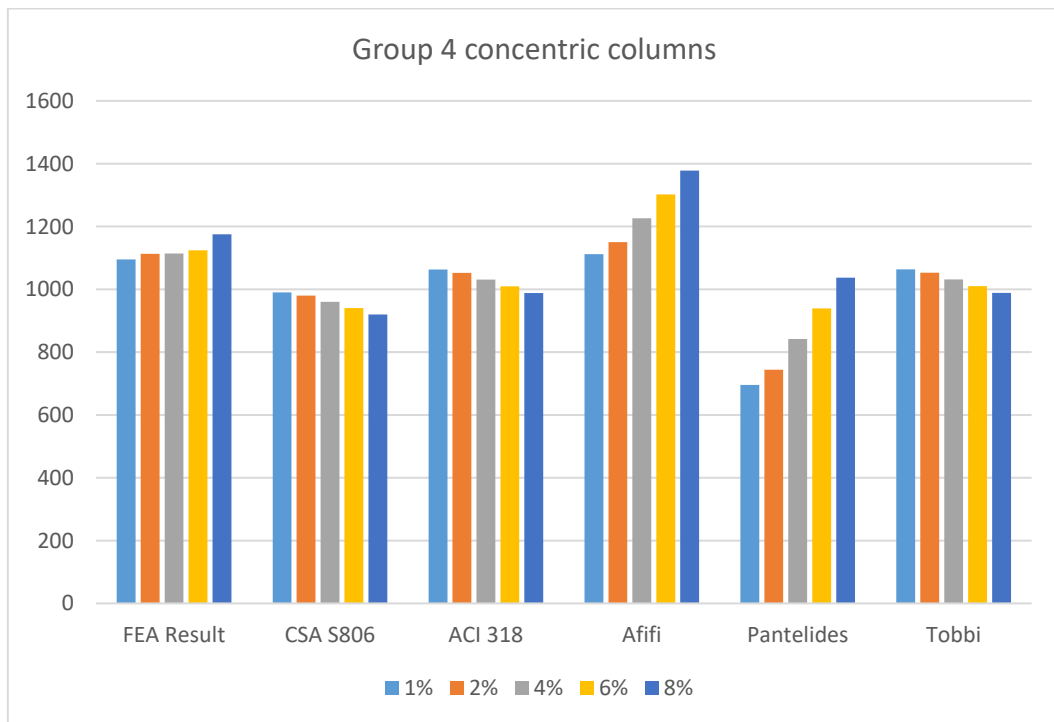


Figure 5.6: Group 4 FEA results comparison with proposed short columns equations

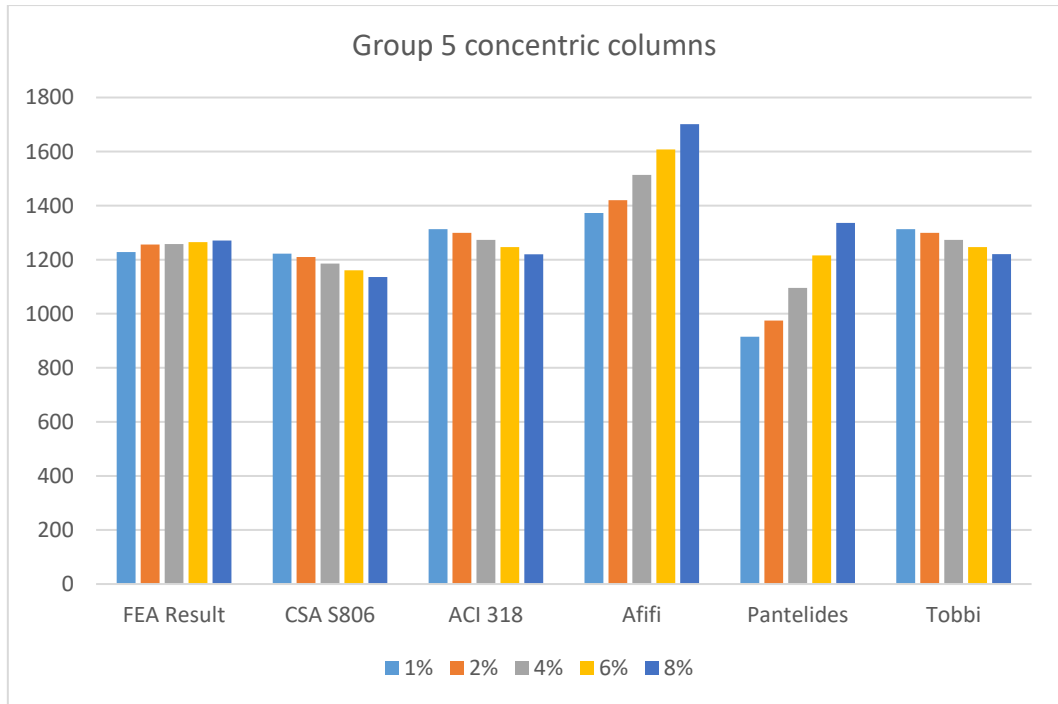


Figure 5.7: Group 5 FEA results comparison with proposed short columns equations

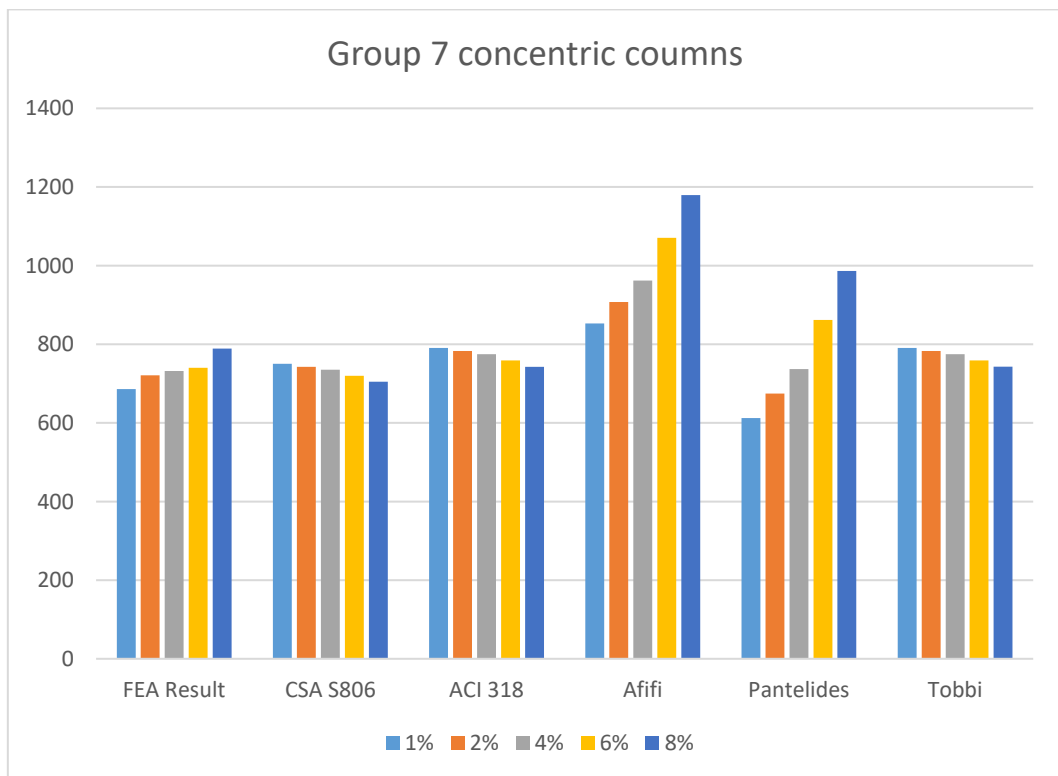


Figure 5.8: Group 7 FEA results comparison with proposed short columns equations

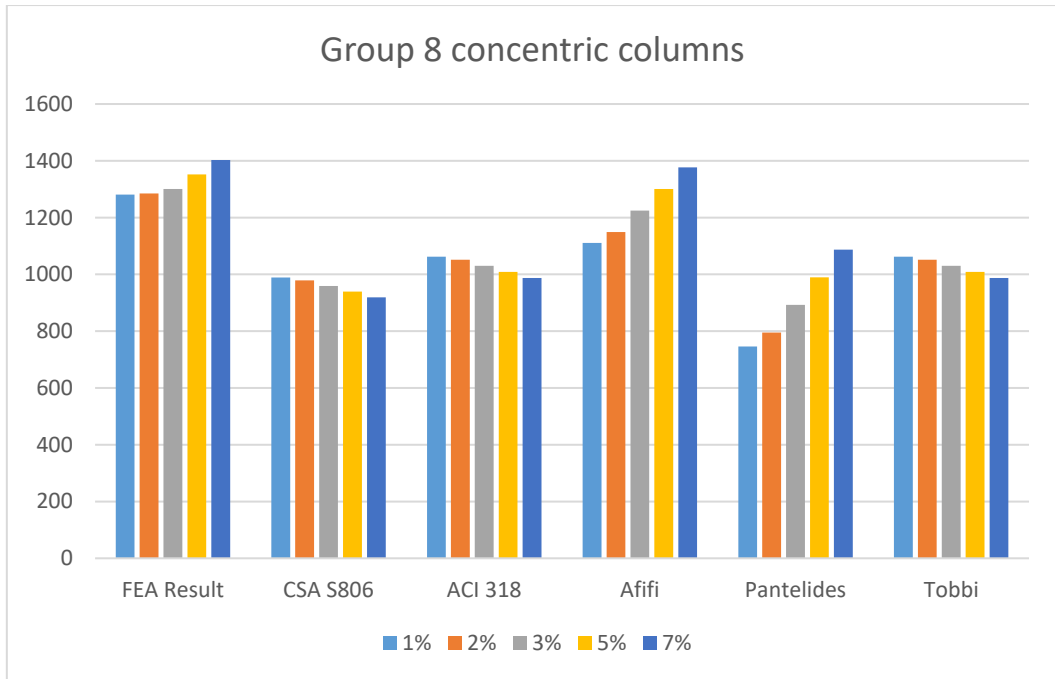


Figure 5.9: Group 8 FEA results comparison with proposed short columns equations

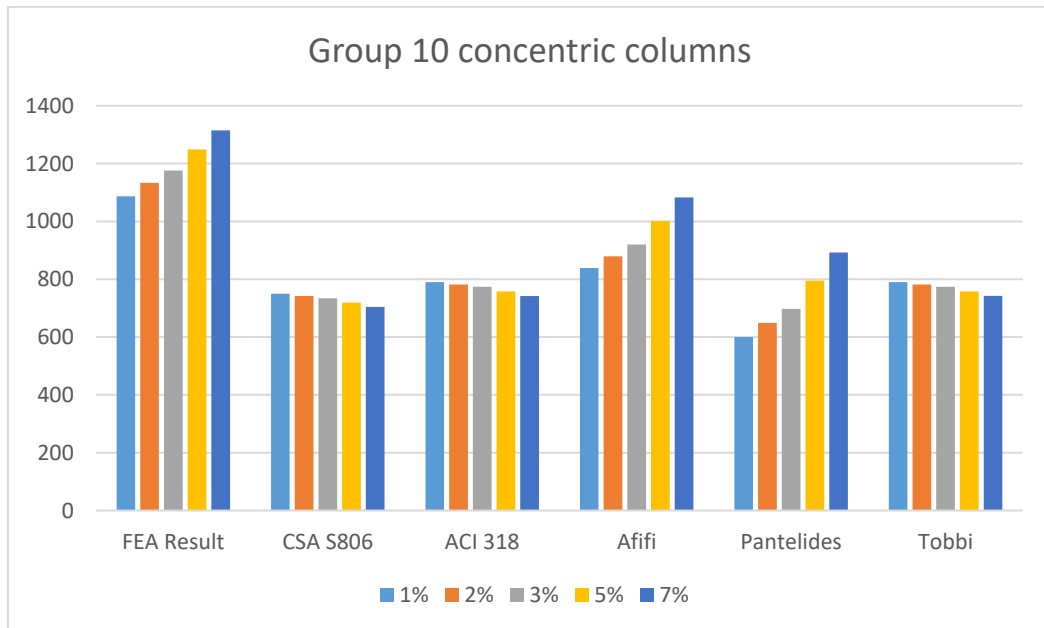


Figure 5.10: Group 10 FEA results comparison with proposed short columns equations

The theoretical equations were compared with the columns in the groups confined with steel reinforcement. It is clear from the comparisons that the CSA S806

[57] and ACI 318 [58] equations, which do not account for the FRP contribution, give lower values than the FEA experimental results, which were, on average, 20% and 13% higher, respectively.

Equation 2. 3 by Afifi et al. [46] overestimates the rectangular column capacity compared to the FEA results, of groups 1 to 7, by an average of 15%. For circular columns, on the other hand, the FEA results showed a higher capacity of around 40%.

Pantelides et al. [47] equation 2. 4 shows a lower estimation of the columns capacity for all groups. It should be noted that the capacity of the columns increases and gets closer to the FEA results with the increase in the reinforcement ratio. The values predicted by the equation, however, were, much lower for the circular columns compared to the FEA results.

Equation 2. 5 by Tobbi et al. [45] showed the most accurate results among all equations, especially for the rectangular columns of groups 1 to 7 with an average difference of 1.6%. The average difference for circular columns, however, was 40% for groups 8 and 10.

Chapter 6. Conclusion and Future Work

In this thesis, the compressive strengths of small and large sizes of GFRP and BFRP bars were examined experimentally under static loads. The experimental results were then utilized as material input to develop nonlinear finite element (FE) models to simulate the axial behavior of concrete columns reinforced with these types of FRP bars. The FE model was initially validated with experimental results on FRP RC columns and then used to conduct an extended parametric analysis to investigate the overall response of FRP RC columns. The parametric analysis included a total of 450 RC columns which were modelled in ABAQUS, including four groups of columns reinforced with GFRP bars and six groups of columns reinforced with BFRP bars. Within these groups, two had BFRP as a transverse reinforcement and one had GFRP as transverse reinforcement. Additionally, three groups had a circular cross section while the remaining seven had a rectangular cross section. The columns were investigated under concentric and eccentric loads as well as the pure-moment case. The test parameters included the longitudinal reinforcement type (GFRP and BFRP), the longitudinal reinforcement ratio (1% to 8%), the transverse reinforcement type (steel, BFRP and GFRP ties or spirals), and the loading eccentricity (0 to 100 mm). The effects of the test parameters on the behavior of the columns were studied in terms of the columns' ultimate capacities, ductility, concrete confinement, and strength contribution of longitudinal reinforcement. The following conclusions can be made from the results of this research:

- The compressive strengths of both GFRP and BFRP bars were much lower than their tensile strength values. Lower compressive strengths were reported for small sized bars than larger sizes.
- There were insignificant differences between columns reinforced with BFRP and columns reinforced with GFRP in terms of overall maximum load, displacement and bars strength contributions.
- The results of the numerical modeling of columns reinforced with GFRP and BFRP bars showed good agreement with the experimental results.
- The capacity and ductility increased when circular cross sections were used for the same cross-sectional area.

- The contribution of main FRP reinforcement generally increased with the increase of reinforcement ratio. The contribution of GFRP and BFRP bars to the ultimate capacities of the columns was found to be ranging from 5% for the lowest reinforcement ratio and up to 30% for higher reinforcement for some sections.
- The ductility of columns reinforced with BFRP or GFRP bars decreased when the reinforcement ratio increased.
- Increasing the longitudinal reinforcement ratio for BFRP and GFRP columns did not significantly affect the ultimate capacities of the columns for concentric columns, but the increase was noticeable for eccentrically loaded columns.
- Using steel ties for confinement of RC columns resulted in higher capacities than using BFRP/GFRP ties, higher concrete core confinement and higher ductility.
- For all load eccentricities, RC columns with steel ties exhibited higher axial load capacities than RC columns with FRP ties. The capacities of steel confined RC columns were higher than those of FRP by around 25 to 40% under concentric loads. However, as the load eccentricity increased, the differences in the ultimate capacities decreased.
- Based on the analytical analysis and experimental study, it is recommended for new codes to consider the contribution of FRP in structural concrete members under compression. The FRP contribution can be included by considering a limited contribution of the total compression capacity of FRP bars.

The review of the literature, and the analysis of the experimental and FEA results have improved the understanding of the structural performance of GFRP and BFRP bars as well as FRP-RC columns; though, additional investigations are essential for an improved understanding of such performance, which can be summarized as follows:

- Few studies have focused on compressive mechanical properties of FRP-RC bars. More tests studied the use of the FRP bars in tension and whether it is needed to limit the contribution of FRP bars in compression.

- Additional experimental and numerical studies are required to further examine the actual contribution of FRP bars in columns under compression, and to actually develop accurate estimation of the capacity of columns reinforced with FRP bars.
- Most of the studies focused on the behavior of GFRP and CFRP bars, while there is still a gap in terms of research about the behavior of BFRP bars.

Finally, using FRP bars to reinforce concrete columns in compression has gained an acceptable behavior. The current design equations are reasonable in predicting the axial capacities of short columns reinforced with FRP for certain material and shapes. Therefore, it seems that it is time to consider the using FRP in compression members in international codes and standards. On the other hand, research should continue investigating more about FRP behavior in compression to reach saturation and to help understand unresolved topics.

References

- [1] S. Chandra Das and E. Haque Nizam, “Applications of Fiber Reinforced Polymer Composites (FRP) in Civil Engineering,” *Int. J. Adv. Struct. Geotech. Eng.*, vol. 03, no. 03, pp. 2319–5347, 2014.
- [2] S. H. R. and T. C. T. C. E. Bakis, L. C. Bank, V. L. Brown, Cosenza, J. F. Davalos, J. J. Lesko, A. Machida, “Fiber-Reinforced Polymer Composites for Construction—State-of-the-Art Review,” *J. Compos. Constr.*, vol. 6, no. 2, pp. 73–87, 2002.
- [3] E. by N. Uddin, *Developments in Fiber-Reinforced Polymer (FRP) Composites for Civil Engineering*. Cambridge: Woodhead publishing Limited, 2013.
- [4] C. Soutis, “Carbon fiber reinforced plastics in aircraft construction,” *Mater. Sci. Eng. A*, vol. 412, no. 1–2, pp. 171–176, Dec. 2005.
- [5] ACI Committee 440, “Guide for the Design and Construction of Externally Bonded FRP Systems for Strengthening Concrete Structures.” ACI 440.2R-02, American Concrete Institute, Farmington Hills, MI, USA, 2008, p. 76.
- [6] L. Van Den Eijnde, L. Zhao, and F. Seible, “Use of FRP composites in civil structural applications,” *Constr. Build. Mater.*, vol. 17, no. 6–7, pp. 389–403, September 2003.
- [7] A. C. 440, *Guide for the Design and Construction of Structural A. C "Guide for the Design and Construction of Structural Concrete Reinforced with Fiber-Reinforced Polymer (FRP) Bars*. American Concrete Institute, 2015.
- [8] U. Berardi and N. Dembsey, “Thermal and Fire Characteristics of FRP Composites for Architectural Applications,” *Polymers (Basel)*, vol. 7, no. 11, pp. 2276–2289, November 2015.
- [9] L. C. Hollaway, “A review of the present and future utilisation of FRP composites in the civil infrastructure with reference to their important in-service properties,” *Constr. Build. Mater.*, vol. 24, no. 12, pp. 2419–2445, December 2010.
- [10] Y. Osugi, R.; Takagi, H.; Liu, K.; Gennai, “Thermal conductivity behavior of

- natural fiber-reinforced,” In *Proceedings of the Asian Pacific Conference for Materials and Mechanics*, Yokohama, Japan, November 2009, pp. 13-16.
- [11] Y. Yao, D. Zhu, H. Zhang, G. Li, and B. Mobasher, “Tensile Behaviors of Basalt, Carbon, Glass, and Aramid Fabrics under Various Strain Rates,” *J. Mater. Civ. Eng.*, vol. 28, no. 9, p. 04016081, September 2016.
- [12] A. El Refai, F. Abed, and A. Altalmas, “Bond Durability of Basalt Fiber–Reinforced Polymer Bars Embedded in Concrete under Direct Pullout Conditions,” *J. Compos. Constr.*, vol. 19, no. 5, p. 04014078, October 2015.
- [13] M. Al Rifai, H. El-Hassan, T. El-Maaddawy, and F. Abed, “Durability of basalt FRP reinforcing bars in alkaline solution and moist concrete environments,” *Constr. Build. Mater.*, vol. 243, p. 118258, May 2020.
- [14] A. Al-Tamimia, F. H. Abed, and A. Al-Rahmani, “Effects of harsh environmental exposures on the bond capacity between concrete and GFRP reinforcing bars,” *Adv. Concr. Constr.*, vol. 2, no. 1, pp. 1–11, March 2014.
- [15] A. Altalmas, A. El Refai, and F. Abed, “Bond degradation of basalt fiber-reinforced polymer (BFRP) bars exposed to accelerated aging conditions,” *Constr. Build. Mater.*, vol. 81, pp. 162–171, April 2015.
- [16] C. Barris, L. Torres, A. Turon, M. Baena, and A. Catalan, “An experimental study of the flexural behaviour of GFRP RC beams and comparison with prediction models,” *Compos. Struct.*, vol. 91, no. 3, pp. 286–295, 2009.
- [17] F. Abed and A. R. Alhafiz, “Effect of basalt fibers on the flexural behavior of concrete beams reinforced with BFRP bars,” *Compos. Struct.*, vol. 215, pp. 23–34, May 2019.
- [18] F. Abed and A. R. Alhafiz, "Finite element simulation of the flexural behavior of BFRP-FRC beams," in *2018 Advances in Science and Engineering Technology International Conferences*, Abu Dhabi, UAE, pp. 1-5.
- [19] H. Alkhraisha, H. Mhanna, N. Tello, and F. Abed, “Serviceability and Flexural Behavior of Concrete Beams Reinforced with Basalt Fiber-Reinforced Polymer (BFRP) Bars Exposed to Harsh Conditions,” *Polymers (Basel)*, vol. 12, no. 9, p. 2110, September 2020.

- [20] A. El Refai and F. Abed, "Concrete Contribution to Shear Strength of Beams Reinforced with Basalt Fiber-Reinforced Bars," *J. Compos. Constr.*, vol. 20, no. 4, p. 04015082, August 2016.
- [21] S. Alhamad, Y. Al Banna, A. Al Osman, J. Mouthasseeb, S. Abdalla, and F. Abed, "Effect of shear span-to-depth ratio on the shear behavior of BFRP-RC deep beams," *MATEC Web Conf.*, vol. 120, pp. 1–8, 2017.
- [22] T. Zhang, D. J. Oehlers, and P. Visintin, "Shear strength of FRP RC beams and one-way slabs without stirrups," *J. Compos. Constr.*, vol. 18, no. 5, 2014.
- [23] F. Abed, H. El-Chabib, and M. AlHamaydeh, "Shear characteristics of GFRP-reinforced concrete deep beams without web reinforcement," *J. Reinf. Plast. Compos.*, vol. 31, no. 16, pp. 1063–1073, August 2012.
- [24] F. Abed, A. El Refai, and S. Abdalla, "Experimental and finite element investigation of the shear performance of BFRP-RC short beams," *Structures*, vol. 20, pp. 689–701, August 2019.
- [25] F. H. Abed, A. Al-Rahmani, and A. H. Al-Rahmani, "Finite element simulations of the shear capacity of GFRP-reinforced concrete short beams," in *2013 5th International Conference on Modeling, Simulation and Applied Optimization (ICMSAO)*, April 2013, pp. 1–5.
- [26] H. Hajiloo, M. F. Green, M. Noël, N. Bénichou, and M. Sultan, "GFRP-Reinforced Concrete Slabs: Fire Resistance and Design Efficiency," *J. Compos. Constr.*, vol. 23, no. 2, pp. 1–13, 2019.
- [27] A. El Refai, F. Abed, and A. Al-Rahmani, "Structural performance and serviceability of concrete beams reinforced with hybrid (GFRP and steel) bars," *Constr. Build. Mater.*, vol. 96, pp. 518–529, October 2015.
- [28] A. Al-Rahmani and F. H. Abed, "Numerical investigation of hybrid FRP reinforced beams," in *proceedings of the 5th International Conference on Modeling, Simulation and Applied Optimization (ICMSAO)*. Hammamet, Tunisia: IEEE; April 2013, pp. 1–6.
- [29] N. Al Huda Tello, M. Abdelrahman, S. El Tonsy, F. Weheda, and F. H. Abed, "Effect of Harsh Environmental Exposure on the Flexural Performance of

- BFRP-RC Beams,” in *2020 Advances in Science and Engineering Technology International Conferences (ASET)*, February 2020, pp. 1–5.
- [30] N. Elmessalami, A. El Refai, and F. Abed, “Fiber-reinforced polymers bars for compression reinforcement: A promising alternative to steel bars,” *Constr. Build. Mater.*, vol. 209, pp. 725–737, 2019.
- [31] V. Plevkov, I. Baldin, K. Kudyakov, and A. Nevskii, “Mechanical properties of composite rebar under static and short-term dynamic loading,” in *AIP Conference Proceedings*, 2017, vol. 1800, no. 1, p.040018: AIP Publishing.
- [32] P. Khorramian, Koosha, Sadeghian, “New testing method of GFRP bars in compression,” in *CSCE Annual Conference 2018*, Fredericton, NB, Canada, Canadian Society for Civil Engineering (2018).
- [33] K. Khorramian and P. Sadeghian, “Experimental and analytical behavior of short concrete columns reinforced with GFRP bars under eccentric loading,” *Eng. Struct.*, vol. 151, pp. 761–773, November 2017.
- [34] D. H. Deitz, I. E. Harik, and H. Gesund, “Physical Properties of Glass Fiber Reinforced Polymer Rebars in Compression,” *J. Compos. Constr.*, vol. 7, no. 4, pp. 363–366, November 2003.
- [35] Q. S. Khan, M. N. Sheikh, and M. N. S. Hadi, “Tension and compression testing of fibre reinforced polymer (FRP) bars,” in *Joint Conference of the 12th International Symposium on Fiber Reinforced Polymers for Reinforced Concrete Structures & The 5th Asian Pacific Conference on Fiber Reinforced Polymers in Structures*, Nanjing, China, 2015, pp. 1-6.
- [36] ASTM D695-10, “Standard Test Method for Compressive Properties of Rigid Plastics,” West Conshohocken, PA 19428-2959: United States, 2010.
- [37] V. P. and R. S. P.Thiyagarajan, “Mechanical Characterization of Basalt Fibre Reinforced Polymer Bars for Reinforced Concrete Structures,” *Res. India Publ.*, vol. 13, no. 8, 2018, pp. 5858–5862.
- [38] J. M. Rotem and A. Lifshitz, “Influence of Strain Rate on the Flexural Properties of a Wood Flour,” in *Proceedings of the 26th Annual Technology Conference*,

Society for Plastics Industry, Reinforced Plastics/Composites Division,
Washington, DC, 1971, pp.1-10.

- [39] F. Abed, Z. Mehaini, C. Oucif, A. Abdul-Latif, and R. Baleh, “Quasi-static and dynamic response of GFRP and BFRP bars under compression,” *Compos. Part C Open Access*, vol. 2, p. 100034, October 2020.
- [40] C. (Canadian S. Association), “Design and construction of building components with fiber reinforced polymers,” Rexdale, ON, Canada, 2012.
- [41] H. A. Hasan, M. N. Sheikh, and M. N. S. Hadi, “Maximum axial load carrying capacity of Fibre Reinforced-Polymer (FRP) bar reinforced concrete columns under axial compression,” *Structures*, vol. 19, pp. 227–233, June 2019.
- [42] A. M. Said, and M. L. Nehdi, “Performance of structural concrete frames reinforced with GFRP grid,” in *13th world conference on earthquake engineering*, Vancouver, B.C., Canada, August 2004, pp. 1679-1691.
- [43] E. D. Szmigiera, K. Protchenko, M. Urbański, and A. Garbacz, “Mechanical Properties of Hybrid FRP Bars and Nano-Hybrid FRP Bars,” *Arch. Civ. Eng.*, vol. 65, no. 1, pp. 97–110, March 2019.
- [44] W. Prachasaree, S. Piriyaakootorn, A. Sangsrijun, and S. Limkatanyu, “Behavior and Performance of GFRP Reinforced Concrete Columns with Various Types of Stirrups,” *Int. J. Polym. Sci.*, vol. 2015, pp. 1–9, 2015.
- [45] H. Tobbi, A. S. Farghaly, and B. Benmokrane, “Behavior of Concentrically Loaded Fiber-Reinforced Polymer Reinforced Concrete Columns with Varying Reinforcement Types and Ratios,” *ACI structural journal*, ” vol. 111, no. 2, pp. 375–386, 2014.
- [46] M. Z. Afifi, H. M. Mohamed, and B. Benmokrane, “Axial Capacity of Circular Concrete Columns Reinforced with GFRP Bars and Spirals,” *J. Compos. Constr.*, ” vol. 18, no. 1, p. : 04013017, 2013.
- [47] M. E. G. and L. D. R. Chris P. Pantelides, S.E., M. ASCE, “Axial load behavior of concrete columns confined with GFRP spirals,” *J. Compos. Constr.*, vol. 17, no. 3, pp. 305–313, 2013.

- [48] N. Nisticò, “R.C. square sections confined by FRP: A numerical procedure for predicting stress–strain relationships,” *Compos. Part B Eng.*, vol. 59, pp. 238–247, March 2014.
- [49] S. H. Lo, A. K. H. Kwan, Y. Ouyang, and J. C. M. Ho, “Finite element analysis of axially loaded FRP-confined rectangular concrete columns,” *Eng. Struct.*, vol. 100, pp. 253–263, October 2015.
- [50] M. Elchalakani, A. Karrech, M. Dong, M. S. Mohamed Ali, and B. Yang, “Experiments and Finite Element Analysis of GFRP Reinforced Geopolymer Concrete Rectangular Columns Subjected to Concentric and Eccentric Axial Loading,” *Structures*, vol. 14, pp. 273–289, June 2018.
- [51] Z. Liu, W., Xu, M., Chen, “Parameters calibration and verification of concrete damage plasticity model of ABAQUS,” *Ind. Constr.*, vol. 44, no. S1, pp. 167–171, 2014.
- [52] A. J. Kappos and D. Konstantinidis, “Statistical analysis of confined high strength concrete,” *Mater. Struct.*, vol. 32, no. 10, pp. 734–748, December 1999.
- [53] F. Abed, C. Oucif, Y. Awera, H. H. Mhanna, and H. Alkhraisha, “FE modeling of concrete beams and columns reinforced with FRP composites,” *Def. Technol.*, February 2020.
- [54] N. Makul, *Applications of bagasse ash in innovative modern concrete*, Berlin: Lambert Academic Publishing, 2008.
- [55] J. J. Biernacki *et al.*, “Cements in the 21st century: Challenges, perspectives, and opportunities,” *J. Am. Ceram. Soc.*, vol. 100, no. 7, pp. 2746–2773, July 2017.
- [56] J. W. I. Vegt, K van Breugel, “Fracture mechanics of concrete and concrete structures,” in *Fracture mechanics of concrete and concrete structures - London Duration*, 2007, pp. 579–587.
- [57] CSA-S806-12, “Design and construction of building structures with Fibre-reinforced Polymers,” Canadian Standards Association, 2012.
- [58] *Building Code Requirements for Structural Concrete and Commentary on*

Building Code Requirements for Structural Concrete, ACI 318-19, 2019.

- [59] (ACI) Committee 440 (2015). “Guide for the design and construction of structural concrete reinforced with fiber-reinforced polymer (FRP) bars. ” ACI 440.1R-15, American Concrete Institute, Farmington Hills, MI, USA.
- [60] L. AlNajmi and F. Abed, “Evaluation of FRP Bars under Compression and Their Performance in RC Columns,” *Materials (Basel)*., vol. 13, no. 20, p. 4541, October 2020.
- [61] N. ElMessalami, F. Abed, and A. El Refai, “Response of concrete columns reinforced with longitudinal and transverse BFRP bars under concentric and eccentric loading,” *Compos. Struct.*, vol. 255, p. 113057, January 2021.
- [62] N. ElMessalami; F. Abed; A. El Refai, “Concrete Columns Reinforced with GFRP and BFRP Bars under Concentric and Eccentric Loads: Experimental Testing and Analytical Investigation,” *ASCE Journal of Composites for Construction*, *In press*, 2021.
- [63] S. Pessiki and A. Pieroni, “Axial load behavior of large-scale spirally-reinforced high-strength concrete columns,” *ACI Struct. J.*, vol. 94, no. 3, pp. 304–314, 1997.
- [64] Amr S. Elnashai and Luigi Di Sarno, *Fundamentals of Earthquake Engineering*, Second Edi. West Sussex: John Wiley and Sons, 2015.
- [65] M. Sargin, S. K. Ghosh, and V. K. Handa, “Effects of lateral reinforcement upon the strength and deformation properties of concrete,” *Mag. Concr. Res.*, vol. 23, no. 75–76, pp. 99–110, September 1971.

Vita

Laith Al Najmi was born in 1990, in Amman, Jordan. He joined the University of Jordan in September 2008, and graduated with a Bachelor's of Science degree in Civil Engineering in February, 2013. After which, he worked in the industry for seven years where he started as a graduate engineer in Petrofac international limited and developed to become a steel connection design specialist where he was engaged in many complicated connections designs.

While he was working in Petrofac, he pursued masters studies in Civil Engineering at AUS, in January, 2018. His research interests are in structural engineering and materials, with particular interest in steel design and connection detailing.